A SINGLE ACTUATOR MODULAR MINIATURE ROBOT CAPABLE OF MANEUVERABLE MULTI-LEGGED LOCOMOTION THROUGH ANISOTROPICALLY ARRANGED SOFT BACKBONES

A THESIS SUBMITTED TO
THE GRADUATE SCHOOL OF ENGINEERING AND SCIENCE
OF BILKENT UNIVERSITY
IN PARTIAL FULFILLMENT OF THE REQUIREMENTS FOR
THE DEGREE OF
MASTER OF SCIENCE
IN
MECHANICAL ENGINEERING

By
Burak ARSLAN
July 2025

A Single Actuator Modular Miniature Robot Capable of Maneuverable Multi-Legged Locomotion Through Anisotropically Arranged Soft Backbones
By Burak ARSLAN
July 2025

We certify that we have read this thesis and that in our opinion it is fully adequate, in scope and in quality, as a thesis for the degree of Master of Science.

Onur ÖZCAN(Advisor)

Salih Özgür ÖĞÜZ

Mehmet Efe TİRYAKİ

Approved for the Graduate School of Engineering and Science:

Orhan Arıkan
Director of the Graduate School

ABSTRACT

A SINGLE ACTUATOR MODULAR MINIATURE ROBOT CAPABLE OF MANEUVERABLE MULTI-LEGGED LOCOMOTION THROUGH ANISOTROPICALLY ARRANGED SOFT BACKBONES

Burak ARSLAN
M.S. in Mechanical Engineering
Advisor: Onur ÖZCAN
July 2025

This thesis presents the design, modeling, and control of a modular miniature robot with a single actuator. The robot has functionally diverse passive legged modules that are connected by anisotropically positioned soft I-beam PDMS backbones. These provide directional compliance and combined with controlled vibration by an unbalanced rotating mass, they allow generating multiple gaits in the legs that cause forward, lateral, and rotational locomotion without the use of additional actuators or added mechanics. A scalar parameter, α, was incorporated to define the orientations of the backbones. It enabled efficient characterization of locomotion at various frequencies of actuation. The robot has a high-fidelity dynamic model in which the flexibility in the backbones was simulated by multi-segmented revolute joint chains. The joint parameters are obtained by performing a series of oscillation experiments in the physical system and optimized using Bayesian optimization. An effectiveness index was assembled based on the system robustness alongside sensitivity to variation in friction. Additionally, the control signals to be applied by the rotation of the system around the robot geometry center, in order to generate 2D locomotion, are learned using a reinforcement learning algorithm. The outcome of the behavior was verified in simulation, and applied to maneuver through a tight path. Overall, this work demonstrates that anisotropic and asymmetric mechanical design, in conjunction with learning-based control, enables adaptive locomotion in underactuated systems using minimal hardware. The outcome instigates the development of compliant robots that can scale for deployment in constrained, alongside unstructured, environments.

Keywords: miniature robots, soft robots, bio-inspired robots, legged robots.

ÖZET

ANIZOTROPIK OLARAK YERLEŞTIRILMIŞ YUMUŞAK OMURGALAR SAYESINDE MANEVRA KABILIYETI YÜKSEK ÇOK AYAKLı HAREKET YAPABILEN, TEK AKTÜATÖRLÜ MODÜLER MINYATÜR ROBOT

Burak ARSLAN
Makine Mühendisliği, Yüksek Lisans
Tez Danışmanı: Onur ÖZCAN
Temmuz 2025

Bu tez, tek bir aktüatörle tahrik edilen modüler bir minyatür robotun tasarımını, modellenmesini ve kontrolünü sunmaktadır. Robot, PDMS malzemesinden üretilmiş, anizotropik olarak yerleştirilmiş yumuşak I-kiriş sırt yapılarıyla birbirine bağlanan, işlevsel olarak farklı bacaklı modüllerden oluşmaktadır. Bu sırt yapıları, yönsel uyumluluk kazandırmakta ve dengesiz dönen bir kütleden kaynaklanan kontrollü titreşimle birleştiğinde, bacaklarda ileri, yanal ve dönme hareketleri gibi çeşitli yürüme desenlerinin ortaya çıkmasını sağlamakta, böylece ilave aktüatörler veya karmaşık mekanik yapılar gerektirmemektedir. Sırt yapıların yönelimini tanımlamak için tek bir skaler parametre olan *alpha* tanıtılmıştır. Yüksek doğrulukta dinamik bir modelolan MuJoCo ortamında geliştirilmiş ve sırt yapılarının esnekliği, çok segmentli döner mafsal zincirleriyle modellenmiştir. Mafsal parametreleri fiziksel salınım deneyleriyle belirlenmiş ve Bayesyen optimizasyon yoluyla hassaslaştırılmıştır. Sürtünme değişikliklerine karşı dayanıklılık ve hassasiyet arasındaki dengeyi değerlendirmek için bir etkinlik indeksi tanımlanmıştır. Buna ek olarak, robotun geometrik merkezinde dönmesini sağlayarak 2B hareketi mümkün kılan kontrol sinyallerini öğrenmek amacıyla bir pekiştirmeli öğrenme algoritması kullanılmıştır. Bu davranış simülasyonda doğrulanmış ve dar bir yol boyunca gezinme görevinde kullanılmıştır.Genel olarak bu çalışma, akıllı mekanik tasarımın öğrenmeye dayalı kontrolle birleştirilmesinin, sınırlı donanıma sahip düşük dereceli sistemlerde uyarlanabilir hareket kabiliyeti sağladığını göstermektedir. Elde edilen bulgular, dar ve yapılandırılmamış ortamlarda çalışabilen, uyumlu ve ölçeklenebilir robotların tasarımına ışık tutmaktadır.

Anahtar sözcükler: minyatür robotlar, yumuşak robotlar, doğadan esinlenen robotlar, bacaklı robotlar.

Acknowledgement

I would like to express my deepest gratitude to Professor Onur Özcan for his invaluable support and guidance, not only during the course of this master's thesis but also throughout my academic journey starting from my early undergraduate years. His mentorship has been instrumental in shaping both my research and career aspirations. I also sincerely thank Professor Daniel M. Aukes for his mentorship and guidance throughout this work.

I would also like to acknowledge the support provided by TÜBİTAK BİDEB under the 2210-A National MSc Scholarship Program, which made this work possible.

My sincere thanks go to all members of the Miniature Robotics Lab for their support and collaboration, especially Ömer Çağrı Ergin, Yiğit Yaman, Altar Sertpoyraz, and Amirali Aleali, whose contributions enriched my experience.

Finally, I would like to extend my heartfelt thanks to Dr. Bengü Akgök and Dr. Uğur Bozüyük for their unwavering support, encouragement, and kindness throughout the writing of this thesis.

Contents

1 Introduction **1**

1.1 Motivation 1

1.2 Literature Review and Research Aims 1

1.3 Structure of the Thesis 4

2 Design **6**

2.1 Conceptual Design 6

2.2 Using Soft I-Beams as Backbones 9

2.3 α Value 12

2.4 Modules 14

2.4.1 Actuator Module 14

2.4.2 Courier Module and Electronics 15

2.4.3 Passive Modules 17

2.5 Backbones 18

3 Modeling **20**

3.1 Backbone Modeling 22

3.2 Complete Robot Model 25

3.3 Parameter Calibration and Validation 25

3.4 Simulation Utility 26

4 Control **30**

4.1 Velocity Control using LQG 31

4.2 Position Control using PID 33

4.3 Summary 34

5 Results **35**

5.1 Continuous Rotation Experiments 35

5.2 Sensitivity and Effectiveness 39

5.3 Reinforcement Learning-Based Navigation 43

5.3.1 Learning Framework and Algorithm Selection 44

5.3.2 State, Action, and Reward Definition 45

5.3.3 Training and Results 46

5.3.4 Navigation Demonstration 47

6 Conclusion and Future Work **49**

6.1 Conclusion 49

6.2 Limitations and Future Work 50

List of Figures

1.1 Overview of the modular miniature robot used in this study, consisting of functionally distinct modules interconnected by anisotropically arranged soft I-beam backbones. 3

2.1 Conceptual design. a) Two modules are connected via a soft backbone oriented at a specific angle. The robot is fixed at the second module and actuated through an unbalanced rotating mass located on the first module, generating a characteristic foot trajectory for the left foot. b) Resulting foot trajectories under various combinations of input frequency and backbone orientation. 8

2.2 Conceptual design. a) Four modules are interconnected via soft backbones arranged with specific orientation differences. The robot is actuated by an unbalanced rotating mass on the first module, producing a distinctive gait pattern. b) Representative gaits resulting from different combinations of input frequency and backbone orientation. 9

2.3 I-beam-shaped backbone manufactured from polydimethylsiloxane (PDMS) with adjustable connection hubs. 10

2.4 Illustration of the actuator module with various backbone angles. 11

2.5 Backbone angle configuration space. An overview of the prototype robot with two different configurations; a) $\alpha = 30°$, and b) $\alpha = 60°$. 13

2.6 Exploded view of the robot showcasing each individual part. . . . 14

2.7 Electronics of the courier module, from left to right: potentiometer sensor, ESP32 module, and DC motor. 16

3.1 Full model of the modular robot in the MuJoCo simulation environment, including soft backbones, rigid modules, and the actuator assembly. 21

3.2 Modeling of the backbone in the MuJoCo environment as a series of 10 mass-spring-damper segments connected along three orthogonal axes: (a) x-axis, (b) y-axis, and (c) z-axis. 22

3.3 Validation of the simulated backbone vibration response against experimental data under a step input: a) x-axis, b) y-axis, and c) z-axis displacements. 24

3.4 Comparison of experimental and simulated trajectories over a 2-second interval for different backbone configurations: a) $\alpha = 0°$; b) $\alpha = 60°$. 28

3.5 Comparison of experimental and simulated trajectories over a 2-second interval for different backbone configurations: a) $\alpha = 90°$; b) $\alpha = 120°$. 29

5.1 Experimental and simulated speed characterization. a) Longitudinal, b) lateral, and c) rotational speed assessments for various actuation frequencies and α values. The leftmost plots show, experimental data with standard deviation values within each cell, the middle column shows simulation results, and the rightmost column shows corresponding percentage errors, respectively. . . . 37

5.2 Simulated effectiveness analysis. a) Longitudinal, b) lateral, and c) rotational effectiveness assessments for various actuation frequencies (x-axis) and α values (y-axis). 41

5.3 Analysis of effectiveness values. a) Trajectory and corresponding gait for $\alpha = 90°$ and $f = 7$ Hz, a configuration associated with high effectiveness. b) Trajectory and corresponding gait for $\alpha = 90°$ and $f = 8$ Hz, a configuration associated with low effectiveness. In both cases, the top panel shows the foot trajectory, while the bottom panel depicts the resulting gait pattern. 42

5.4 Optimal signals for rotation around the center of geometry determined using reinforcement learning for $\alpha = 90$. The y-axis represents the angular position of the mass, corresponding to the control input, while the x-axis denotes time. 47

5.5 A nine-frame sequence illustrating the robot's navigation through a planar maze using a hybrid control strategy. In images 1–4 and 6–7, the robot advances using open-loop straight-path locomotion by alternating between 7 Hz and –7 Hz frequencies. Upon encountering narrow corners, the robot transitions to reinforcement-learning-based rotation maneuvers to realign itself with the path: a right turn in image 5 and a left turn in image 8. Image 9 shows the robot resuming forward motion. 48

List of Tables

2.1 Backbone orientation angles for different α values 14

5.1 Hyperparameters used for PPO training 45

Chapter 1

Introduction

1.1 Motivation

Recently, under-actuated compliant systems have gained substantial attention within the field of soft robotics. These systems make use of the intertwined stiffness and damping properties inherent in their structural design and materials, allowing researchers to develop various robots capable of functions like movement and grasping. What sets these systems apart is their capacity to minimize the need for active actuation by harnessing the dynamic responses of their own physical structure. As a result, they can lower controller complexity, decrease the number of required actuators, and streamline the overall fabrication process.

1.2 Literature Review and Research Aims

Under-actuated compliant systems are thus a focal area of interest for soft robotics for reasons related to relieving pressures on actuation and on control. Scholars have investigated specially crafted metamaterials and mechanics that enable soft systems to adopt both sensing [1–3] and actuation roles [4, 5]. Incorporating the former philosophies into soft robots further extends their capabilities for getting beyond actuation and control hurdles. Classical soft robotic systems, by virtue of being highly deformable, nonlinear in characteristics, and high degrees of liberty, are tendental in needing voluminous configurations for actuation to obtain preferred operations. In such regards, this creates barriers in accurately modeling motion for controlling it precisely. Through investigation and incorporation on the properties of materials as well as on structural dynamics, scholars have been able to craft new soft robots with capabilities for movement [6,7], grasping [8–10], manipulating [11,12] objects with lowered reliance on active actuation. These also include prospects for designing robots less complex to create and cost-competitive for prospects for large-volume fabrication for purposes such as swarm robotics or operations in hostile environments.

Significant legged robot developments span the size range from meters [13–16] to centimeters and even millimeters [17–20]. While such robots offer unparalleled agility, they invariably need more than 10 actuators for efficient functioning. The over-reliance causes complications due to supply of power, modeling the system, as well as controlling it, thus driving up cost and labor for manufacturing. In overcoming such shortcomings, scientists have had to fall back on methods to permit legged robots motion using fewer actuators. Through the addition of mechanical linkages as well as curvature to structures [21–23] they are capable of obtaining preset gait patterns for permitting rapid motion using minimal actuation input. Besides, self-stabilizing passive walking robots [24, 25] have come into existence whose design positions them to obtain locomotion using lesser actuators. Even so, while capable of showing motion using lesser actuation input efficiently, such systems are usually capable of supporting fewer than two distinct movement modes due to restricted gait range thus overall restricted versatility for efficient functions.

Actuation mechanisms for legged robots for the past couple of decades have remained a major area of interest. A wide range of technologies has come up for consideration, ranging from the more conventional DC motors to gear pair-based brushless motors and dedicated actuation technologies available for centimeter- [26] and millimeter-scale [27] robots in the form of pneumatic setups, tendon-based configurations, and piezoelectric actuation [28]. While efficient in driving robotic motion, however, such approaches tend to depend on having a dedicated actuator for individual legs, thereby increasing complexity in the design of the robot and making it more challenging to control. Vibration actuation has thus come into play as a potential option for addressing such factors. Its greatest virtue lies in the fact that vibrational forces can easily be distributed over the robot's overall structure such that leg motion becomes achievable without the need for individual-leg-mounted separate actuators. A single vibrator actuator located in the center can thus be adequate in driving the system. The approach has achieved success in millimeter-scale legged robots [29–34] in achieving crawling motion through the deployment of slip-stick mechanics. However, while effective in demonstration in movement, such approaches are normally restricted to millimeter-scale robots due to inherent limitations inherent in such actuation energy.

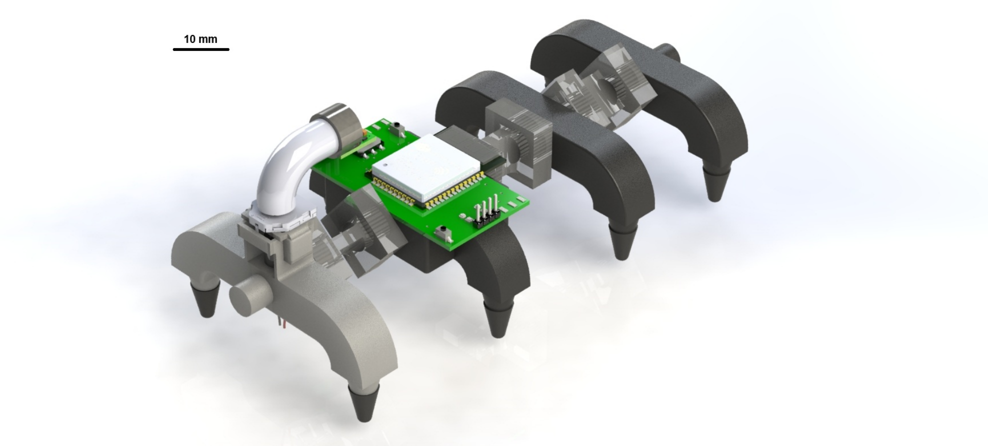

Figure 1.1: Overview of the modular miniature robot used in this study, consisting of functionally distinct modules interconnected by anisotropically arranged soft I-beam backbones.

Unlike previous approaches, this study combines coupled compliant mechanisms with vibration actuation to create a lightweight, centimeter-scale robot equipped with eight legs. The system is powered by a single DC motor that spins an unbalanced mass, serving as the vibration source. Thanks to this design, the robot is capable of performing four distinct types of movement: forward locomotion, turning, and lateral (sideways) translations. A key feature of the robot is the inclusion of soft backbones placed between its modules, which transmit the vibrational energy produced by the rotating mass in the first module. These backbones, which can be fabricated from PDMS, help lower both the manufacturing costs and the complexity of assembly. This work aligns with a new category of devices known as Soft Curved Reconfigurable Anisotropic Mechanisms (SCRAMs), previously explored in systems such as pinched tubes [35–37], buckling beams [38, 39], and twisted beams [40]. Although the individual backbones in this study are not intrinsically curved, the system as a whole, comprising anisotropically arranged soft I-beam backbones, exhibits the functional behavior of a SCRAM. By leveraging the geometry and material characteristics of soft components, the system can streamline complex actuation demands into simplified signals that still generate sophisticated motion.

1.3 Structure of the Thesis

This thesis is structured into six major chapters where each one addresses a crucial aspect of the design, modeling, control, and evaluation of the modular miniature robot.

Chapter 1 introduces motivation, scope, and thesis contributions. It articulates the key challenges in achieving maneuverable locomotion with underactuated miniature robots and formulates the objectives that guide the work.

Chapter 2 provides an introduction to the system architecture and mechanical design for the robot. It describes the working roles for the different modules, anisotropic structure of soft I-beam backbones made up of PDMS, and how compliance permits different gaits with minimal actuation.

Chapter 3 describes the construction of the high-fidelity dynamic simulation model using the MuJoCo physics engine. It describes how backbone flexibility is modeled through multi-segment revolute joints, how experimental oscillation data is used for parameter estimation, and how Bayesian optimization is utilized for the enhancement of simulation fidelity.

Chapter 4 introduces the control scheme utilized for the unbalanced spinning mass driving the robot. It illustrates the structure and implementation of the inner-loop Linear–Quadratic–Gaussian (LQG) controller for the intended velocity tracking as well as the utilized Proportional–Integral–Derivative (PID) controller for position control. A brief introduction on the theory of control and how it is connected with modular robotic systems is also provided.

Chapter 5 characterizes the robot's locomotion across actuation frequencies (±6–8 Hz) and backbone configurations ($\alpha = 0°$, $60°$, $90°$, $120°$), using both experiments and MuJoCo simulations. The results confirm multidirectional movement and validate the simulation accuracy, especially at higher frequencies. A sensitivity analysis was performed by varying surface friction, and an *effectiveness index* was introduced to identify configurations that combine high speed with robustness. Optimal performance was observed at $\alpha = 90°$, $f = 7$ Hz. Finally, a reinforcement learning (PPO) policy was trained to achieve center-of-geometry rotation. The learned strategy was integrated with open-loop forward control to demonstrate full 2D maze navigation, showing that complex motion can be achieved with a single actuator and fixed configuration.

Chapter 6 concludes the thesis by summarizing the overall results and contributions. It also indicates the limitations of the system today and proposes some potential directions for the future, such as adaptive control for unstructured situations, exploration of wider configuration spaces, and scaling the concept to other application domains.

Chapter 2

Design

The robot presented in this work belongs to a broader class of mechanical systems referred to as Soft, Curved, Reconfigurable, Anisotropic Mechanisms (SCRAMs). This category includes mechanisms that derive their complex behavior from the intrinsic geometry and material compliance of soft structures. Previous research has explored such systems through diverse examples such as pinched tubes, buckling beams, and helically twisted elements. These systems share a common feature which is leveraging structural and material anisotropy to simplify actuation and enable novel locomotion or motion behavior without relying on complex jointed mechanisms.

2.1 Conceptual Design

The presented design builds on this principle through a modular robot composed of rigid 3D printed bodies connected via elastomeric I beam-shaped soft backbones. These I beam shaped backbones are the key of the system as their geometric profile offers distinct stiffness properties about the three principal axes of rotation. This anisotropic stiffness distribution is important because it allows the robot to realize directionally tunable compliance, which is fundamental to how locomotion is achieved.

In its most basic form, the robot can consist of two rigid modules interconnected by a single soft backbone. The first module houses an unbalanced rotating mass, which serves as the single actuator for the system. The second module is fixed during the the characterization experiments to isolate the effect of the soft connection and better observe behavior of the legs.of the legs. When actuated, the rotation of the mass induces vibrations that propagate through the soft backbone and manifest as oscillatory motion at the extremities of the structure, most notably at the tips of the legs. Because the backbone is anisotropically arranged, the resulting motion is not symmetrical or linear but instead follows a curved, repeating trajectory at the contact point with the ground. This behavior emerges due to the combined effects of geometric asymmetry and elastic deformation and plays a central role in generating forward or directional movement once the feet interact with a surface.

Specifically, it is seen that small variations in the unbalanced mass rotation frequency, with no other change in the robot, can lead to significant variation in the final motion gait patterns and leg trajectories. These kinds of variation offer a large variety of motion patterns where many are capable of providing controlled multidirectional motion. Therefore, tuning by frequency becomes a critical device for gait generation in this robot structure.

In Fig. 2.1, a robot is presented consisting of two modules connected by a single soft I beam, known as a backbone. We chose I-beam-shaped backbones because of their distinct stiffness characteristics around the three rotational axes, which allows for directionally tunable compliance. The robot is fixed at the rear end of the second module and actuated via an unbalanced mass located on the first module. The generated vibrations travel through the anisotropically arranged backbone, producing an oscillatory response at the tips of the robot's legs. Due to the geometric asymmetry and compliant structure, this results in a curved, repeating trajectory at the feet (shown with dashed blue lines). When in contact with the ground, this motion transforms into a more complex and directional

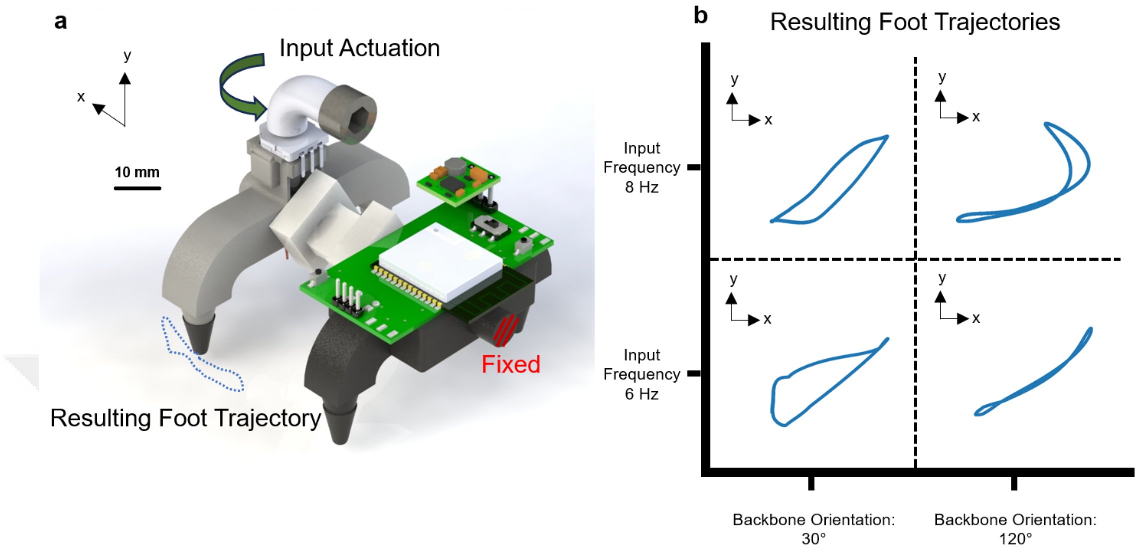

Figure 2.1: Conceptual design. a) Two modules are connected via a soft backbone oriented at a specific angle. The robot is fixed at the second module and actuated through an unbalanced rotating mass located on the first module, generating a characteristic foot trajectory for the left foot. b) Resulting foot trajectories under various combinations of input frequency and backbone orientation.

locomotion. Furthermore, simply increasing the frequency of oscillation significantly alters these trajectories, resulting in a wide range of motion patterns that enable controlled multidirectional locomotion.

Though the two-module structure is predominantly utilized for testing rudimentary gait comportments and foot trajectories amid a significantly simplified world, the system is easily scalable. A four-module extension adds soft backbones structured in I beam form, deployed anisotropically once again. Under this layout, the requirement for some kind of outside tethering is eliminated while providing for planar motion such that the robot is able to maneuver within 2D worlds using a single actuator. Relative backbone disparities between the modules as well as for the soft backbones themselves, parameterized in our system using a single parameter α, are responsible for defining the resultant gait's form as well as directionality. Changes in both the actuation frequency as well as backbone angle disparities lead to the robot having the capability for performing an extensive range of gait types, shown in Fig. 2.2, responsible for creating versatile navigation as well as mobility for a host of specific roles.

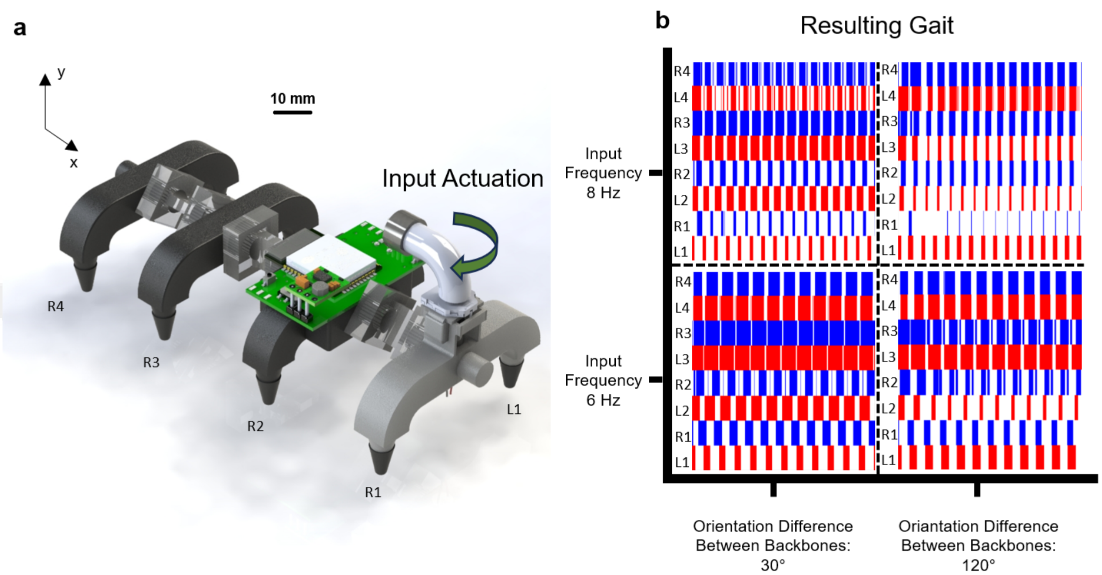

Figure 2.2: Conceptual design. a) Four modules are interconnected via soft backbones arranged with specific orientation differences. The robot is actuated by an unbalanced rotating mass on the first module, producing a distinctive gait pattern. b) Representative gaits resulting from different combinations of input frequency and backbone orientation.

2.2 Using Soft I-Beams as Backbones

The backbones are fundamentally one of the most critical components in the robot's design, enabling both mechanical connectivity and directional motion shaping. In our system, three identical soft I-beam-shaped backbones are used to interconnect four rigid modules. These backbones were made from polydimethylsiloxane (PDMS) using a 7: 1 base-to-curing-agent weight ratio through a custom molding process. The choice of PDMS at this ratio was motivated by its reliable flexibility, consistent curing behavior, and mechanical stability, which together allow for repeatable deformation under vibratory loads. Fig. 2.3 showcases the computer aided design drawing of a single backbone.

Figure 2.3: I-beam-shaped backbone manufactured from polydimethylsiloxane (PDMS) with adjustable connection hubs.

Structurally, I-beam form has anisotropic stiffness properties whose values are high about the web axis, intermediate about the flange, and low in torsional about its longitudinal axis. As such, it is an ideal candidate for robotic systems where directionally tunable compliance is a requirement. In our system, we achieve such directional compliance to convert symmetric vibrational input due to an individual spinning unbalance into asymmetric curved motion on the legs whose result is efficient locomotion.

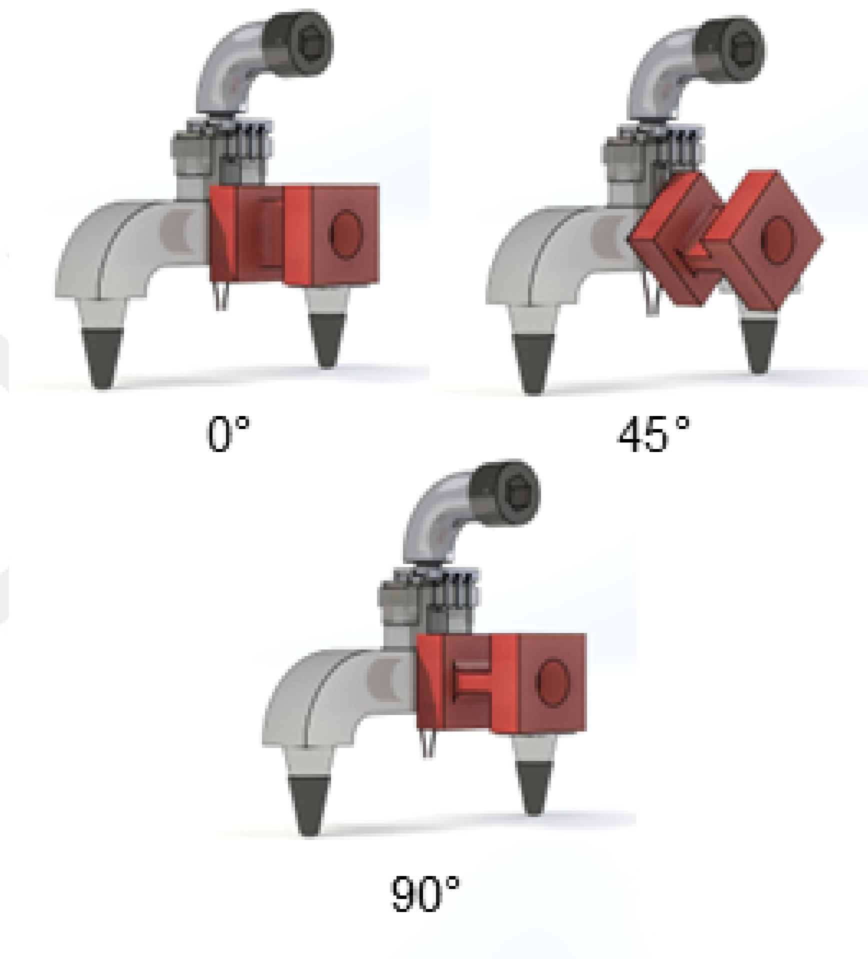

Figure 2.4: Illustration of the actuator module with various backbone angles.

PDMS backbones are used to interconnect proximate modules built out of polylactic acid (PLA), 3D printed for modularity and precision. A cylindrical coupling mechanism is used for implementing all interfaces between the backbones and the modules. The coupling not just provides for safe bonding but also provides a handy feature: it permits immediate reconfiguration of the robot layout by simple variation in the angle between the backbone and the individual module. Such variability is indispensable for our work since it allows for efficient experimentation with practically any backbone orientation and robot structure directly affecting gait diversity and efficiency.

By reorienting the relative angles between individual modules and corresponding I-beam backbone structures, we basically change the overall robotic body's net anisotropy. Changing such angle-dependent reorientations of stiffness axes redistribute vibrations input throughout the structure differently, thus varying overall robot dynamic response. Such angular alignments are an additional tuning parameter, as is frequency, controlling resultant motion patterns as well as locomotion modes. The above is the essence of our approach in providing fine-grained tuning for gait characteristics without hardware modification or additional actuation.

With the integration of soft I-beam-shaped PDMS backbones with tunable cylindrical couplings, the system achieves an ideal trade-off between modularity, reconfigurability, and mechanical compliance. In the process, it transforms a simple single input actuation into sophisticated multidirectional locomotion patterns without employing complicated control algorithms or more than one actuator.

2.3 α Value

Since individual backbone angles may arise from a continuous collection $[-90°, 90°]$, the sheer number of possible combinations renders extensive experimental verification impractical. To account for this issue, we describe the angle configuration through one parameter, α. The backbone angles are then assigned as α, 2α, and 3α. Some possible configurations for $\alpha = 30°$ and $\alpha = 60°$ are depicted in Fig. 2.5. Parametrization significantly minimizes the design space such that the system's behavior may be explored experimentally and computationally efficiently.

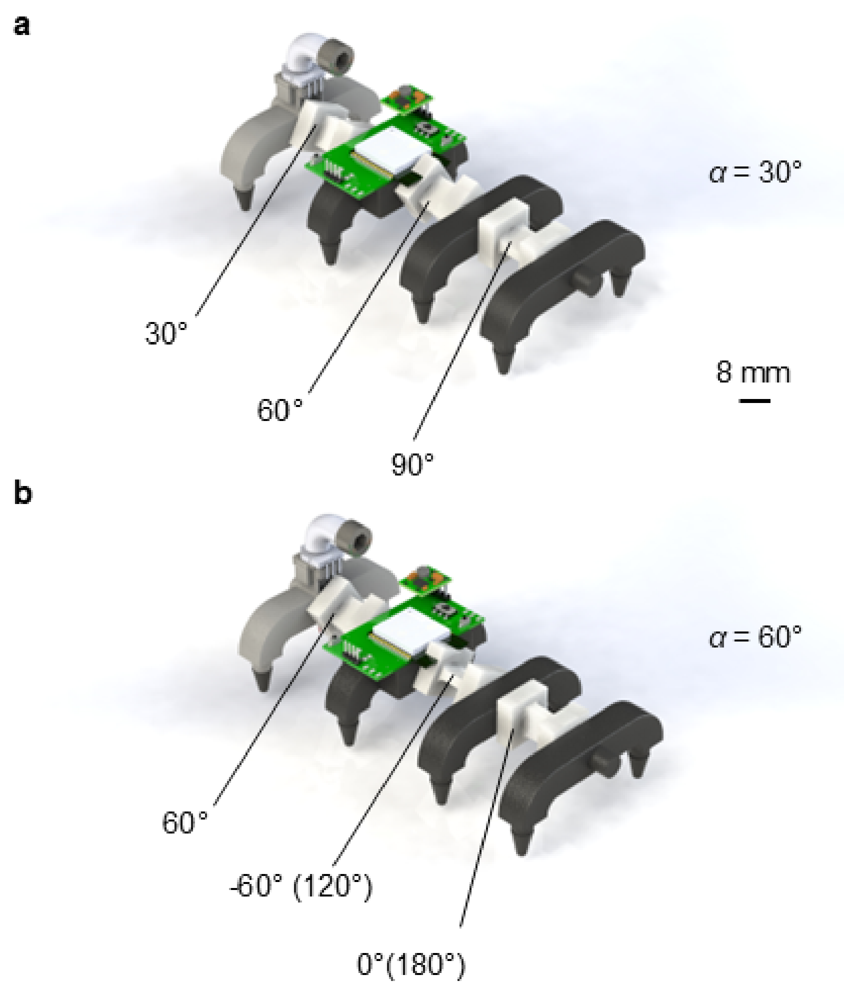

Figure 2.5: Backbone angle configuration space. An overview of the prototype robot with two different configurations; a) $\alpha = 30°$, and b) $\alpha = 60°$.

In the experimental section of this study, four different backbone configurations were analyzed, corresponding to α values of 30°, 60°, 90°, and 120°. The associated backbone orientations are summarized in Table 2.1.

Table 2.1: Backbone orientation angles for different α values

α (deg)	**Backbone 1**	**Backbone 2**	**Backbone 3**
30	30	60	90
60	60	120	180
90	90	180	270
120	120	240	360

2.4 Modules

All robot modules are 3D printed using PLA and designed with integrated footpads, manufactured from soft silicone, to enhance surface grip and friction for balanced and repeatable locomotion. The robot comprises three distinct types of modules which are actuator, courier, and passive, each contributing a unique function to the overall locomotion strategy while sharing a common centipede-inspired geometry. An overview of the design is given in Fig. 2.6.

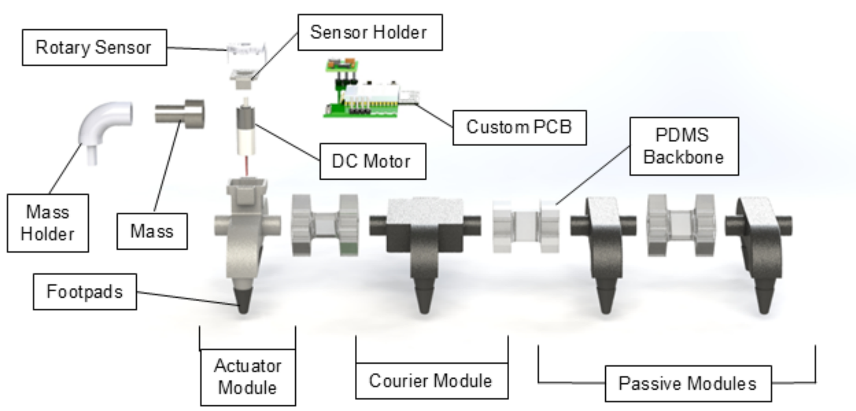

Figure 2.6: Exploded view of the robot showcasing each individual part.

2.4.1 Actuator Module

The first module of the robot is called the actuator module. Like the other modules, it is designed in the form of a single centipede-like unit, with two legs attached symmetrically. What distinguishes the actuator module from the passive modules (described in the following section) is the presence of an onboard actuator: a 26:1 Sub-Micro DC Motor (Pololu, NV, USA), mounted vertically at the center of the module body, perpendicular to the ground.

A custom 3D-printed extension is fixed to the shaft of the motor. This extension carries a 3 mm aluminum bolt, which serves as an unbalanced mass and generates periodic vibrations when the motor rotates. The geometry of this component affects two critical parameters simultaneously: the radius of rotation of the unbalanced mass, defined as the horizontal distance from the motor shaft center, and the height of the mass, measured vertically from the module surface. Both of these values influence the input vibration transmitted to the backbone that connects the actuator module to the adjacent courier module. This vibratory input directly affects the resulting leg trajectory and gait pattern of the robot.

In all experiments conducted in this study, the unbalanced mass and the 3D-printed component remained fixed, with a rotation radius of X mm and a height of X mm from the surface of the first module. To enable precise control over the rotational speed—and therefore the amplitude and frequency of vibration, a rotational position sensor (Model 3382, Bourns, CA, USA) is used. This sensor allows for closed-loop control of the motor's angular velocity.

2.4.2 Courier Module and Electronics

The second robot module is also referred to as the courier module. In design, it is a mirror image of the passive modules' geometry and leg arrangement, with the one distinction being that the body width is doubled so more electronics and power equipment can fit. With the larger volume, it is capable of accommodating the heart of the control and communication system.

A bespoke printed circuit board (PCB) is affixed to the module and holds the major electronics. The core is the ESP32-WROOM-32 microcontroller unit (MCU)

(Espressif Systems, China), which powers the control logic as well as radio communication. The MCU supports ESP-NOW, a low-footprint but secure wireless communication protocol providing low-latency data exchange between modules as well as outside-in systems of control such that untethered real-time operation is possible.

The PCB is equipped with two rotational position sensor hubs (Model 3382, Bourns, CA, USA), current implementation uses one such hub to sense the velocity and position of the mass. These are interpreted by the MCU to establish the appropriate control outputs. The MCU sends instructions to a motor driver (L293DD, STMicroelectronics), based on the data, which powers the robot via a 1:136 Sub-Micro DC Motor (Pololu, NV, USA). Fig. 2.7 illustrates the key components.

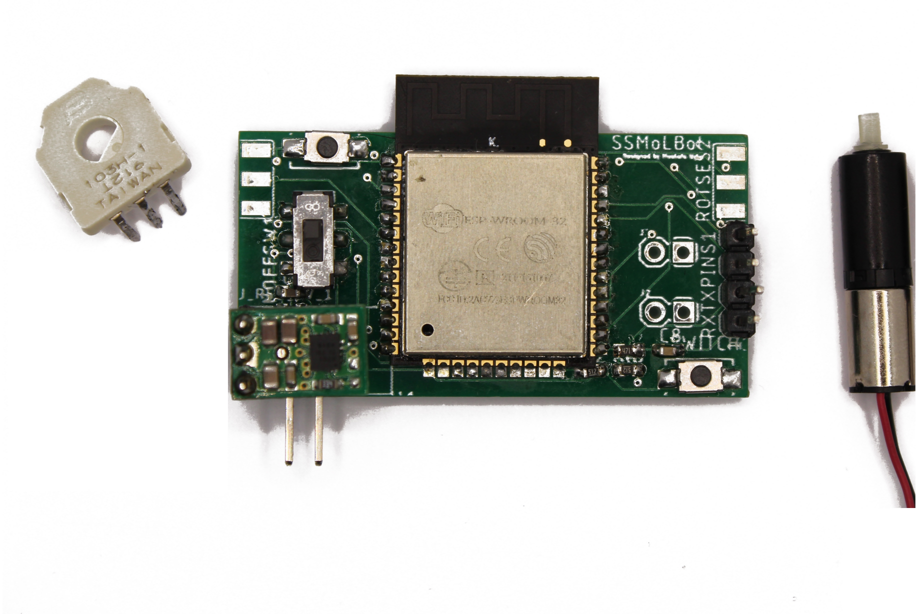

Figure 2.7: Electronics of the courier module, from left to right: potentiometer sensor, ESP32 module, and DC motor.

To power the system, a 3.7V 150 mAh single-cell Li-Po battery (JJRC, China) is mounted on the underside of the courier module. A step-up regulator (S7V7F5, Pololu) increases the voltage to 5.0V, supplying the motor driver and DC motor, while a step-down regulator (NCP1117, Onsemi) provides 3.3V to the MCU and sensors. This dual-regulator setup ensures appropriate power delivery to all components.

The module also includes programming pins that enable the reconfiguration of the embedded code when needed. This design ensures flexibility for adapting to new control strategies, updated feedback logic, or communication routines during development.Through this hardware setup, the courier module not only transmits actuation commands but also processes sensor data.

2.4.3 Passive Modules

Passive modules are responsible for the conversion of the vibration energy conveyed through the soft backbone into leg motion. Passive modules are unique compared to actuator and courier modules by the fact that they carry no motors or on-board electronics. Passive modules also rely exclusively on the robot's compliance properties as well as geometric structure in order to generate foot motion and maintain locomotion.

Each passive module is also identical to the actuator in mechanical design apart from the part where the sensor is located. They essentially act to carry over the result of the input vibration induced by the actuator module by using the additional soft backbones connected together in series between the modules. The motion output at the legs of each passive module is regulated by the anisotropic deformation of the backbone together with the resonant properties of the module.

For this thesis work, the configuration was standardized to two passive modules for four total modules (actuator, courier, and two passive). We chose this configuration as a fair trade-off between locomotion efficiency and simplicity of control. Experimentally, we also observed that additional passive modules increase more friction as well as mechanical resistance, particularly near the feet. Therefore, motion tends to result in more rotational motion about the last (rear) module than balanced translational gait. The reason for this is that more passive modules result in more ground contact forces as well as dissipate less energy into motion in the forward direction.

Passive module design ensures modularity and scalability for the robot architecture. Two passive modules were utilized in this work, but the system is readily extendible or reconfigurable for study of many other gaits or motion strategies by varying the quantity or structure of passive segments accordingly for the input motion.

2.5 Backbones

These compliant backbones are the key feature in the design of our robot for transferring vibrations and permitting anisotropic deformation between connected modules. To create the work for this purpose, we fabricated three identical backbones from polydimethylsiloxane (PDMS) mixed in base to cure agent ratio 7:1 and cast into custom 3D printed molds. There are a number of reasons why this choice is perfect for our application. PDMS is chemically stable and biocompatible such that it is capable for repeated dynamic deformation. Due to low glass transition temperature and superior resistance to fatigue, it is ensured to maintain mechanics properties for long-term cyclic loading. What is more, the stiffness of PDMS easily could be controlled by using the mixing ratio or cure conditions such that it is particularly perfect for the fabrication of backbones with application-defined compliance.

Each backbone joins two consecutive modules by a circular cylindrical coupling mechanism such that it is simple to rapidly experiment and fine-tune the robot's anisotropic response by varying the backbone orientation. Varying the angle between consecutive modules directly varies the directional stiffness profile of the robot so as to modify the manner vibrations are transmitted as well as how foot trajectories are produced, thereby altering the resultant gait.

I-beam cross-section was selected for the backbone midsection due to the directionally dependent stiffness properties. The I-beam structure has more resistance to bending and twisting about specific axes such that orientation-dependent tunable compliance is permitted for. With the inherent structure anisotropy in the I-beams themselves, the robots' dynamic properties are predictable both by the actuation frequency and by the spatial backbone configuration.

Care was also taken in choosing the backbone lengths so as to balance structure integrity with avoidance of collision between modules during large-amplitude oscillations. With such design, modularity and versatility are achieved for the robot with mechanical stability during movement.

Chapter 3

Modeling

A simulation environment was built to study and predict the motion of the modular miniature robot for an extremely large range of backbone structures and actuation conditions. The physics engine used for this is MuJoCo (Multi-Joint Dynamics with Contact) [41], which is a high-speed simulator with a focus on model-based control, optimization, and physics-informed machine learning.

MuJoCo also has some distinct advantages compared to standard rigid-body simulators. Differing from engines where graphics realism is emphasized more, MuJoCo is built from the ground up for speed and for precise simulation of physics interactions. It also supports soft and compliant bodies via tendon, spring, and damping models and can handle high-frequency actuation and collisions with time steps as low as submillisecond. Contact dynamics are also efficiently handled in MuJoCo via a convex optimization-based approach. That enables stable and precise simulation for complex contact situations such as foot-ground contact for legged robots.

Another advantage is that it offers user-defined joint types, actuator models, and fine-grained control over body form and physical characteristics. These are exactly the capabilities best adapted for simulating contact between deformable structures — like the soft backbones used by this robot — with rigid bodies,

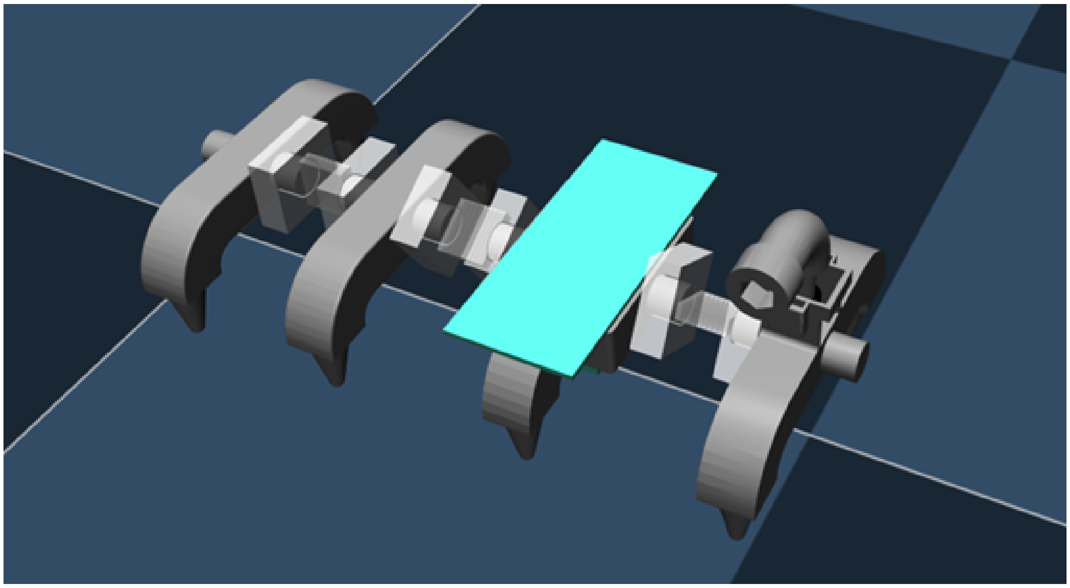

Figure 3.1: Full model of the modular robot in the MuJoCo simulation environment, including soft backbones, rigid modules, and the actuator assembly.

frictional surfaces, and moving loads like oscillating eccentric masses.

Additionally, MuJoCo is integrated with Python using the mujoco-py library such that it is possible to utilize contemporary reinforcement learning libraries such as Stable-Baselines3 and run parameter optimization routines. The simulator also has real-time rendering capabilities, batch simulation, and intrinsic sensors for monitoring forces, joint states, and contact dynamics such that it serves as an effective utility for both model validation as well as control development.

MuJoCo was utilized to design a high-fidelity robot model comprising soft backbones, rigid modules, and one actuator with a moving eccentric mass. A summary is shown in Fig. 3.1. Simulations were constructed to mimic both compliant backbone deflection as well as complex interaction between actuation due to vibration and resultant robot motion. A detailed account is included in the following sections on how compliance in the backbone was simulated, how experimental data was utilized in calibration of physical parameters, as well as how the complete robot model was compared to real-world measurements for verification.

3.1 Backbone Modeling

To accurately model the compliant behavior of the soft backbones, each backbone was segmented into 10 evenly spaced rigid elements connected via revolute joints along the x, y, and z axes, enabling three-dimensional oscillations as demonstrated in Fig. 3.2. The backbone structure, therefore, consists of 30 revolute joints, where each axis-specific joint type shares a common set of stiffness and damping parameters. This design allows the backbone to deform dynamically in response to vibrations induced by the unbalanced rotating mass.

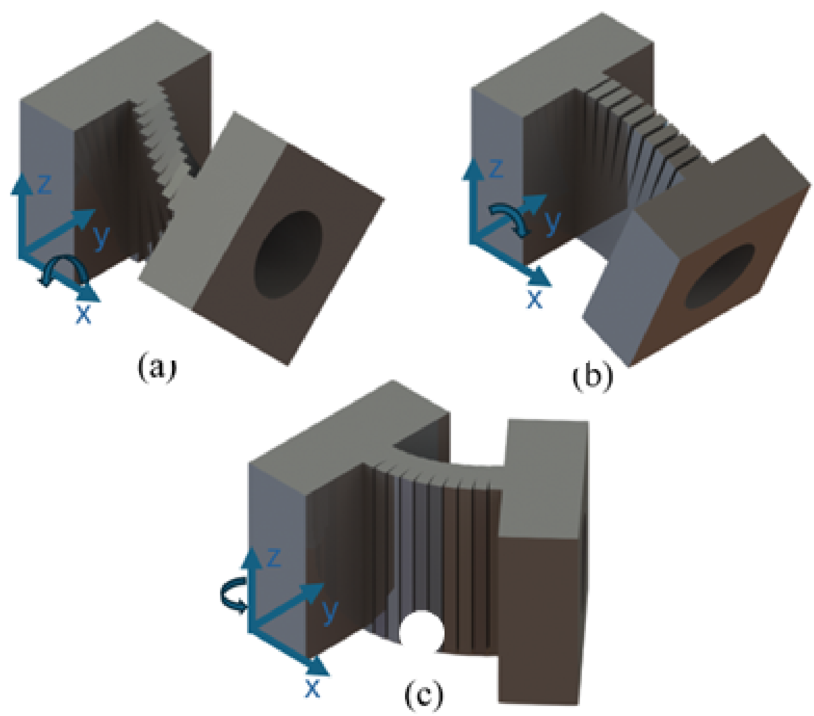

Figure 3.2: Modeling of the backbone in the MuJoCo environment as a series of 10 mass-spring-damper segments connected along three orthogonal axes: (a) x-axis, (b) y-axis, and (c) z-axis.

For physical fidelity, the stiffness (k) and damping (d) values for each axis were empirically determined through controlled oscillation experiments. In each test, the backbone was manually displaced along one axis and released, and its oscillatory response was recorded using a motion capture system. These responses were then replicated in a simplified MuJoCo model containing only one axis of deformation at a time.

To extract accurate stiffness and damping parameters, a Bayesian optimization algorithm was used to minimize the root mean square error (RMSE) between the experimentally measured and simulated trajectories. The cost function was defined as:

$$J = \sqrt{\frac{1}{T}\sum_{t=1}^{T} \|\boldsymbol{\theta}_{\mathrm{sim}}(t) - \boldsymbol{\theta}_{\mathrm{exp}}(t)\|^2} \tag{3.1}$$

where $\boldsymbol{\theta}(t)$ denotes the angular orientation of backbone segments at time t in simulation and experiment, respectively. This yielded six independent parameters: stiffness and damping for each of the x, y, and z axes. The comparison between the experimental and simulated responses of each backbone axis to a step input is presented in Fig. 3.3.

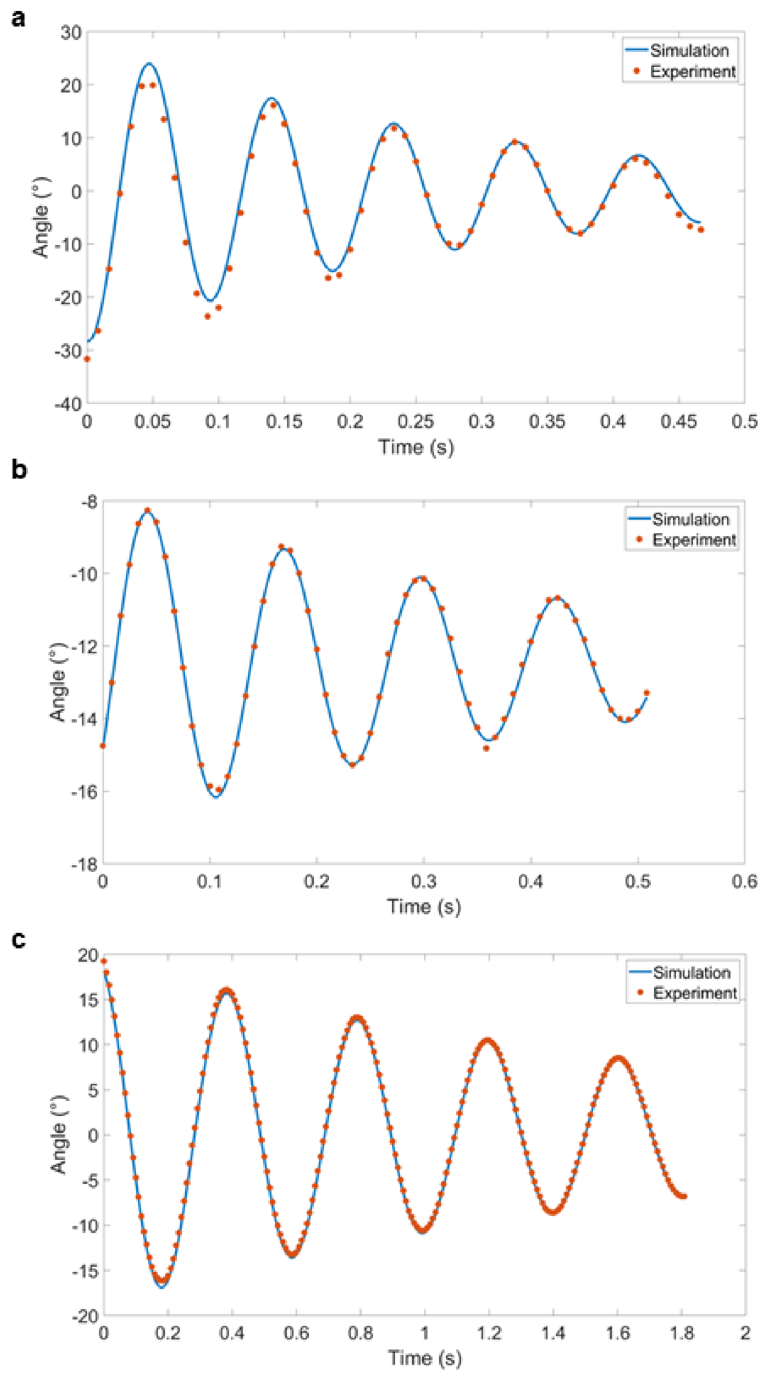

Figure 3.3: Validation of the simulated backbone vibration response against experimental data under a step input: a) x-axis, b) y-axis, and c) z-axis displacements.

3.2 Complete Robot Model

The total robot structure consists of four rigid modules (actuator and courier module included) plus three soft backbones and one rotor with offset mass. The backbones are represented segment-wise by the above calibrated segment-wise model with ten segments for each backbone and joint-based compliance on the revolute joints. Rigid modules are represented by STL meshes with assigned physical parameters such as to match the actual prototype in terms of mass, inertia, and geometrical properties.

A cylindrical eccentric mass is also connected to an actuator module's motor shaft to mimic the actuation mechanism. The eccentric load has a simulated height, radius, and mass distribution according to prototype readings. A sinusoidal input is used to rotate such an eccentric mass around a balance spot to achieve locomotion through the resultant vibration-induced forces transmitted by the backbones.

The ground is estimated to be a static frictional plane, and friction coefficients for contact points were fine-tuned to consider contact between robot legs and experimental surface. The simulation is initialized with a timestep of 10^{-4} s to observe high-speed dynamic interactions.

3.3 Parameter Calibration and Validation

The simulation parameters are calibrated using experimental trajectory data collected from actual experiments conducted under a set of actuation frequencies ($f = \{-8, -7, -6, 6, 7, 8\}$ Hz) and backbone angle configurations ($\alpha = \{0°, 60°, 90°, 120°\}$). A motion capture system was utilized to retrieve the robot's positional and angular trajectories for comparison with the simulation output for the identical input conditions.

A second optimization procedure was then used after the identification of the overall parameters to improve the simulation's accuracy. In this procedure, joint stiffness and damping factors were varied along each of the three principal directions so as to get a total of six parameters. Furthermore, coefficients of friction in each foot–ground contact location were adjusted to more accurately match experimental interactions, while rotor-related parameters like impedance and reference acceleration were also optimized. All these optimizations enabled the simulation to emulate realistically the actual system behavior of the robot for a wide range of backbone configurations as well as actuation profiles.

The optimization objective was updated to minimize the aggregate error in the average forward, lateral, and angular velocities:

$$\mathcal{L} = \sum_{i} |V_{\mathrm{exp},i} - V_{\mathrm{sim},i}| \tag{3.2}$$

where V_i denotes the average speed in one of the three motion components. The final model demonstrated strong agreement with the physical prototype, accurately reproducing the observed trajectories across all tested configurations. Each experimental condition was repeated three times, and the resulting trajectories were compared with the corresponding simulation outputs, as shown in Fig. 3.4 and Fig. 3.5.

3.4 Simulation Utility

The MuJoCo model verified is also a key ingredient for some significant aspects of this work. Firstly, it is utilized for predicting gait and trajectory patterns for backbone configurations never experimented with physically, thereby permitting iteration in the design space quickly without labor-intensive experimentations. Secondly, it is utilized for sensitivity analyses by simulating how locomotion is affected by surface friction or variation in actuation parameter through simulations, thereby permitting determination of stable and robust operating points. Finally, the MuJoCo environment is the platform for simulation on reinforcement learning, particularly for deriving navigation policies where controlled rotation of center-of-geometry is necessitated by the robot.

The high fidelity of the simulation ensures the transferability of the virtually implemented control strategies and behaviors to the real robot with reliability. That transferability maintains low requirements for extensive re-tuning or redesigning as one moves from simulation to hardware, so the simulation environment is invaluable for design exploration as well as for control development.

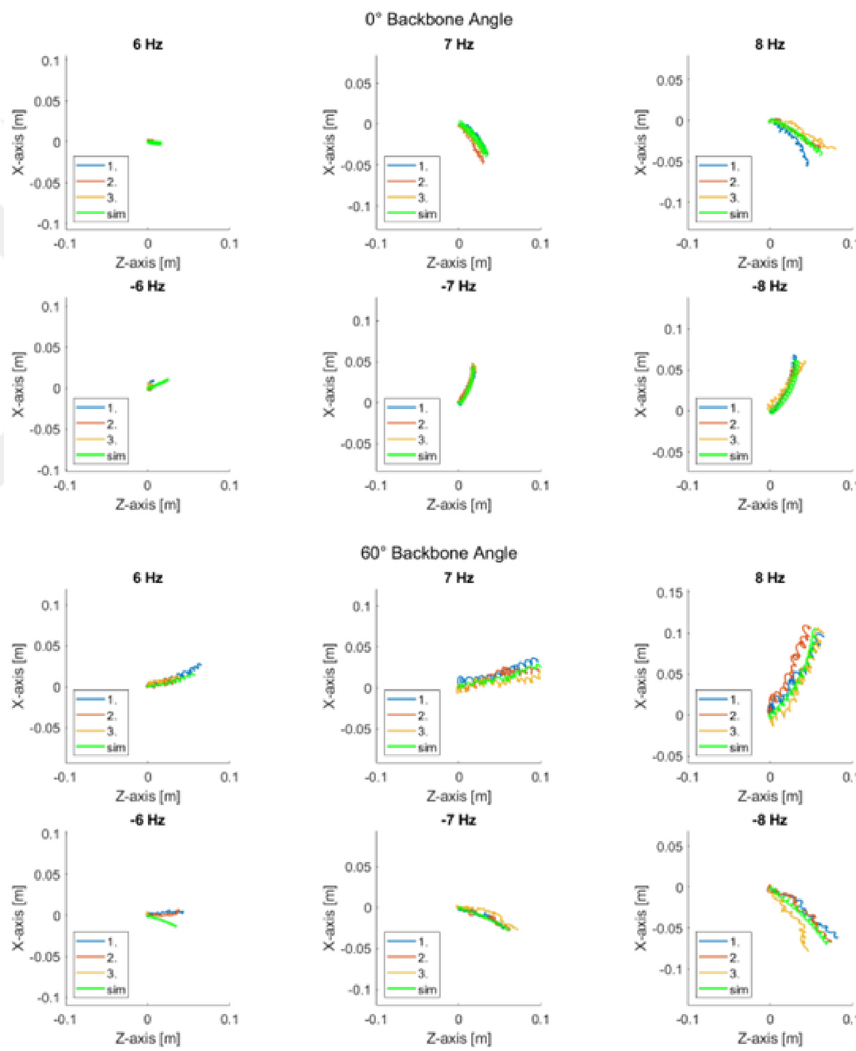

Figure 3.4: Comparison of experimental and simulated trajectories over a 2-second interval for different backbone configurations: a) $\alpha = 0°$; b) $\alpha = 60°$.

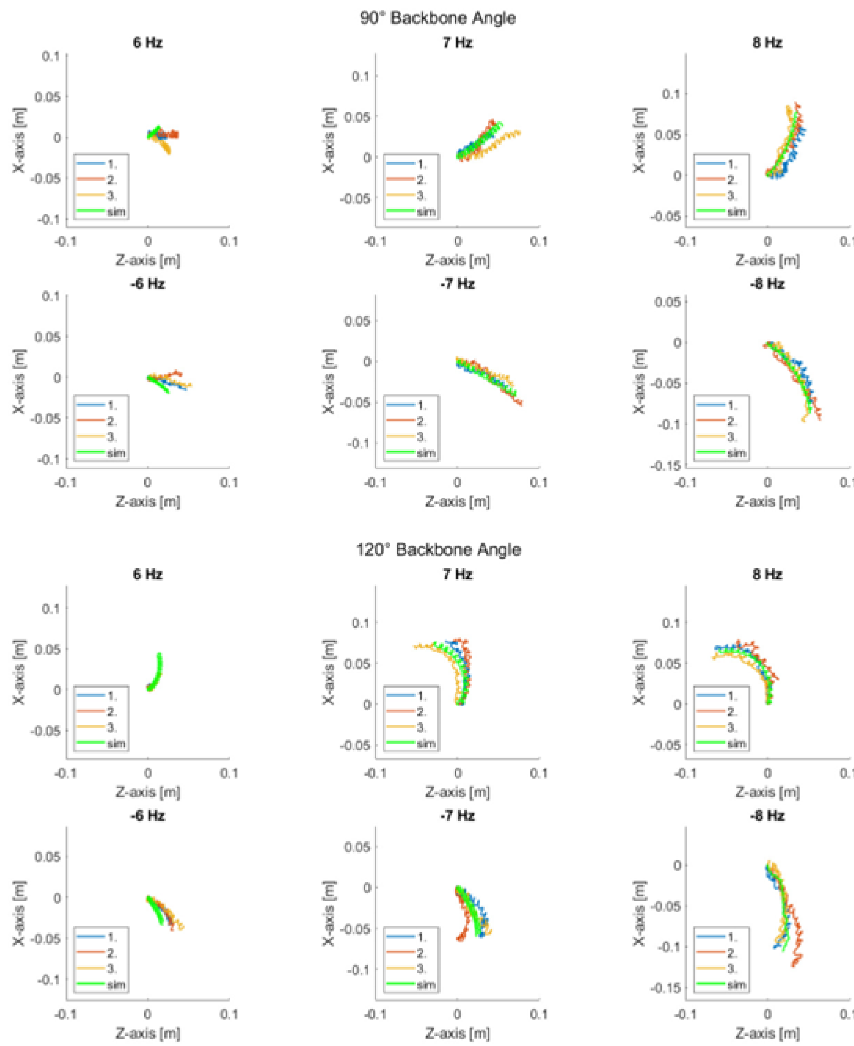

Figure 3.5: Comparison of experimental and simulated trajectories over a 2-second interval for different backbone configurations: a) $\alpha = 90°$; b) $\alpha = 120°$.

Chapter 4

Control

Control for robotic systems is the actuation of an input signal such that one is able to achieve a desired dynamic response within the hardware. For most conventional robots such as wheel vehicles or manipulator arms, regulatory techniques are employed for wheel speed, joint locations or joint trajectories. Most such systems are developments on the basis of stiff actuation mechanisms and numerous sensors for receiving the feedback. But for our robot, it adheres to a completely different principle of movement: all movement is achieved by one unbalanced mass whose spin creates the mechanical vibrations. These vibrations are transmitted by soft anisotropic backbones, which ultimately lead to movement.

For the system we are considering, standard trajectory following or gait scheduling techniques are not appropriate. What is in fact controllable is the rotational motion of the unbalanced mass or the angular velocity or angular position. The motion and contact with the world by the robot is a consequence of how this spinning mass is distributing mechanical energy throughout the structure. So defining low-level controllers for the unbalanced mass becomes critical for designing and switching effective gait patterns.

To meet various experiment design goals, two distinct methods of control are used. When it is desirable to achieve steady high-frequency vibrations to drive locomotion at a specified constant frequency, a Linear Quadratic Gaussian (LQG) controller is used to regulate the angular velocity of the mass. When it is desirable for the motion to change between angular positions or assume a characteristic orientation (e.g., for oscillatory motion), a Proportional-Integral-Derivative (PID) controller is utilized to directly regulate the angular position of the mass. These controllers are employed for specific but complementary roles and are executed on the robot's onboard microcontroller. The selection between them is done based on the nature of the concerned task if one is required for frequency-stable actuation or position-based control is desirable. The two approaches are described in the following sections along with the mathematical models and implementation considerations built into the system.

4.1 Velocity Control using LQG

When the goal is to maintain a specific rotational frequency of the unbalanced mass, we employ an LQG controller. The LQG architecture combines a Linear Quadratic Regulator (LQR) with a Kalman Filter-based state estimator (LQE). This enables accurate regulation of the motor speed despite limited sensor feedback and system noise.

The rotational dynamics of the DC motor is modeled using Kirchhoff's voltage law and Newton's second law:

$$v = Ri + L\frac{di}{dt} + K_e\omega \tag{4.1}$$

$$J\frac{d\omega}{dt} = K_t i - b\omega \tag{4.2}$$

Here, v is the applied voltage, i is current, ω is angular velocity, R is armature resistance, L is inductance, K_e is the back emf constant, K_t is the torque constant, J is the moment of inertia, and b is the damping coefficient.

The system is represented in a state-space form with the state vector:

$$\boldsymbol{x} = \begin{bmatrix} \theta \ \omega \ i \end{bmatrix} \tag{4.3}$$

The control objective is to track a desired angular velocity ω (specified via frequency f), with phase $\theta(t) = \beta_0 + 2\pi f t$ and reference current i_{free}. The reference vector is:

$$\boldsymbol{r} = \begin{bmatrix} \beta_0 + 2\pi f t \ 2\pi f \ \ i_{\text{free}} \end{bmatrix} \tag{4.4}$$

The control input is generated by:

$$\boldsymbol{u} = \mathbf{K}(\boldsymbol{r} - \hat{\boldsymbol{x}}) \tag{4.5}$$

The $\mathbf{K}$ matrix is computed using LQR optimization that minimizes the cost function:

$$J = \int_0^\infty !(\boldsymbol{x}^\top \mathbf{Q} \boldsymbol{x} + \boldsymbol{u}^\top \mathbf{R} \boldsymbol{u}), dt \tag{4.6}$$

where $\mathbf{Q}$ and $\mathbf{R}$ are weight matrices chosen using Bryson's Rule. A Kalman filter estimates the full state $\hat{\boldsymbol{x}}$ from noisy position measurements using different noise covariance matrices depending on whether the sensor is operating in a reliable zone or the dead zone (around $[-15°, 15°]$).

This hybrid LQG structure allows us to accurately control rotational frequency even when sensor quality degrades in certain angular regions.

4.2 Position Control using PID

In some experiments, instead of tracking a continuous rotational velocity, the robot is required to move to or oscillate between specific angular positions (e.g., for back-and-forth oscillatory behaviors). In this case, a PID controller is used rather than the LQG controller.

The PID controller operates based on the angular error:

$$e(t) = \theta_{\text{target}} - \theta(t) \tag{4.7}$$

The control signal is computed as:

$$u(t) = K_p e(t) + K_i \int e(t)dt + K_d \frac{de(t)}{dt} \tag{4.8}$$

where K_p, K_i, and K_d are the proportional, integral, and derivative gains, respectively. In our system, we often use only proportional control ($K_i = K_d = 0$) to maximize responsiveness, especially for fast transitions between two angular boundaries.

To suppress sensor noise and improve stability, a moving average filter is applied to position readings prior to error calculation. Additionally, the controller logic includes logic to switch direction when angular limits are reached, enabling continuous oscillation between two predefined angles.

This PID-based control loop is particularly useful in scenarios where a fixed-speed rotation is not necessary and direct position control offers more effective interaction with the environment.

4.3 Summary

Briefly, the system constructed in this research is able to work in two modes, optimized for specific situations during the locomotion experiments. A Linear Quadratic Gaussian (LQG) controller is employed where stable continuous frequency control of the unbalanced mass is required, providing accurate tracking of the objective angular velocity through model-based state estimation. A Proportional-Integral-Derivative (PID) controller is employed where angular boundaries are either static or where oscillatory motion between pre-defined boundaries is mandatory. The former mode allows efficient direction switching and is simpler to implement. Both controllers are executed on a microcontroller in real time with the mode chosen dynamically according to the desired locomotion behavior.

Chapter 5

Results

Locomotion for the robot starts when the actuation frequency is above 5 Hz. Thus, in order to identify the nature of locomotion for the robot as well as evaluate the performance of our digital simulation, we did continuous rotation experiments for various backbone angle configurations and compared the results with those from our simulation.

5.1 Continuous Rotation Experiments

We performed experiments by actuating the robot at fixed frequencies for a duration of 2 seconds. The actuation frequencies were chosen as $f = \{-8, -7, -6, 6, 7, 8\}$ Hz and were combined with four different backbone configurations defined by $\alpha = \{0°, 60°, 90°, 120°\}$, resulting in a total of 24 unique test cases. These frequency values were selected in line with actuator limitations: the robot starts performing locomotion around 5 Hz, and its maximum stable frequency is around 9 Hz. We chose simple continuous rotation for 2 seconds to clearly identify the system's behavior and establish a consistent benchmark for comparison with simulation results.

Each experiment was repeated three times. For all trials, we assessed the final longitudinal, lateral, and rotational speeds, and compared them against the respective speeds computed with the MuJoCo model. The simulation vs. experiment error for all cases was computed using the normalized percentage error equation:

$$\varepsilon = \frac{V_{\text{sim}} - V_{\text{exp}}}{\max(|V_{\text{exp}}|)} \tag{5.1}$$

where V_{sim} is the simulated speed and V_{exp} is the corresponding experimental measurement. This error metric was applied independently for each speed component.

The results are visualized in Figure 5.1. In both experimental and simulation plots, blue regions indicate positive speeds and red regions indicate negative speeds. The results demonstrate that the robot is capable of achieving both positive and negative longitudinal, lateral, and rotational velocities, confirming that multidirectional maneuvering is possible with a single actuator.

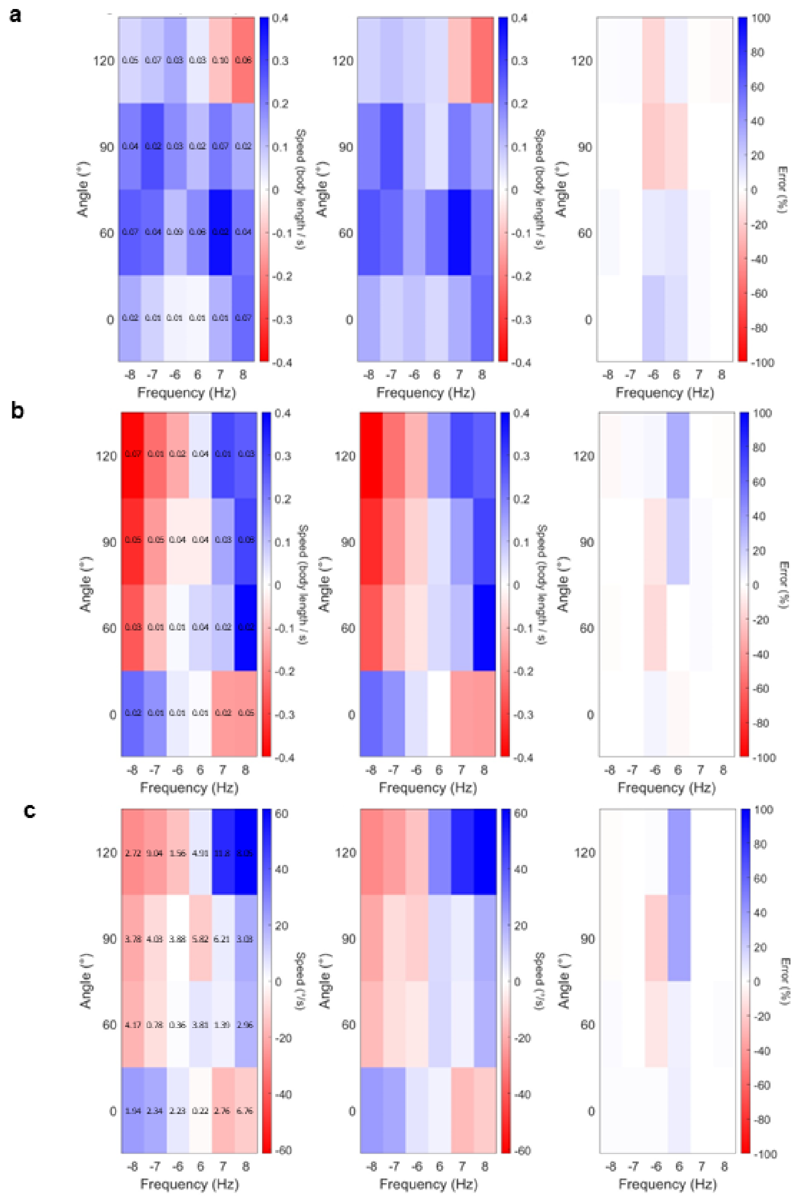

Figure 5.1: Experimental and simulated speed characterization. a) Longitudinal, b) lateral, and c) rotational speed assessments for various actuation frequencies and α values. The leftmost plots show, experimental data with standard deviation values within each cell, the middle column shows simulation results, and the rightmost column shows corresponding percentage errors, respectively.

The simulation is in good agreement with the experimental data, particularly at frequencies of ± 7 and ± 8 Hz, where the model error is virtually nil. That would mean the digital model is doing a good job simulating the system dynamics for high-speed conditions. But for ± 6 Hz, up to about a 20% maximum deviation was observed. That discrepancy is most likely due to increased frictional phenomena for low-speed conditions where the model fails to adequately include it. These results show the model is reliable for high-frequency conditions but must be improved for low-speed conditions to include low-speed friction phenomena.

These foot trajectory traces from the recorded data also provide additional evidence on the influence on resultant gait patterns by different backbone angles and actuation frequencies. For $\alpha = 0°$, the traces are relatively circular and axisymmetric, evidencing low directionality bias and more balanced vibration dispersal over the robot. Then for increasing backbone angle to 60°, 90°, and 120°, the traces are more elongated and curved in shape with more directionality and more distinct locomotion behaviors.

In all configurations with non-zero α, the robot consistently tends towards the left when the unbalanced mass is rotated in the clockwise direction (positive frequencies) and rightward under counterclockwise rotation (negative frequencies). This asymmetry stems from the way the anisotropic backbones transmit vibration differently depending on their orientation and the direction of input rotation as designed. Also, as α increases, this turning bias becomes more prominent, particularly at higher frequencies (7–8 Hz), where the amplitude of the foot trajectories is larger and more consistent.

The simulation outputs (marked in green) align well with the experimental paths and validate that the model effectively captures the direction-dependent dynamics induced by the soft, anisotropically arranged backbones. Minor deviations at lower frequencies can be attributed to the unmodeled physical factors such as surface friction variability or mechanical tolerances. Moreover, we would also hope for results to be very close, if not exactly the same, for $\alpha = 0°$ and $\alpha = 90°$, considering the system is highly symmetric, particularly in simulation. In experimental scenarios in the real world, the results deviate because of manufacturing tolerances and the imperfections of the surface topography. In simulation, however, the nonsymmetry is introduced almost entirely by the courier module, not being perfectly symmetric and having an uneven weight distribution given the placement of the components including the battery and the voltage converter. Moreover, we also introduce controller noise as well as actuation noise in the simulation so that we better capture the conditions in the real world and introduce more variation.

5.2 Sensitivity and Effectiveness

For obtaining reliable as well as stable locomotion in potentially uncertain surface configurations, we investigated effectiveness as well as sensitivity by varying the environment in friction. The motivation for this work originates in the fact that even though a robot appears effective for locomotion in nominal conditions, small shifts in surface properties—the sorts of which include friction—can significantly influence speed, sturdiness, as well as general robot behavior. Therefore, it is desirable to obtain operating configurations not only for effectiveness in speed in locomotion but also for sturdiness for such variations. These are desirable for obtaining reliable functioning.

In order to attain this, we performed a sensitivity analysis by varying the friction coefficient in the simulation by 10% and observing how the speed response of the robot was altered. Simulations were performed in MuJoCo using the same backbone angle and frequency combinations as during the above rotation experiments. For every setting, percentage change in velocity due to the varied friction coefficient was calculated. The thus calculated percentage change, denoted by the sensitivity σ, is an indication of how sensitive the robot's locomotion is to environmental perturbations in surface properties. The sensitivity is mathematically represented as:

$$\sigma = \left| \frac{V_f - V_i}{V_i} \right| \tag{5.2}$$

where V_i is the initial velocity under nominal friction conditions, and V_f is the velocity after increasing the friction coefficient by 10%. A lower σ value implies that the configuration is less sensitive to changes in surface friction and therefore more robust.

It is important to note that configurations yielding zero velocity (i.e., the robot remains stationary) inherently exhibit the lowest sensitivity values, as there is no measurable change in speed regardless of the friction variation. However, these configurations are not useful from a locomotion perspective. To identify configurations that are both fast and stable, we define an effectiveness index, φ, which combines the robot's speed performance with its sensitivity to frictional changes. This metric enables the identification of optimal operation points where the robot achieves high speed with minimal sensitivity. The effectiveness index is defined as follows:

$$\varphi = |V| \left(1 - \frac{\sigma}{\sigma_{\max}}\right) \tag{5.3}$$

V is the speed achieved for a given configuration, σ is the corresponding sensitivity, and $\sigma_{\max}$ is the largest observed value for the corresponding speed type (longitudinal, lateral, or rotational). Normalizing σ in such a way keeps the index within bounds and comparable from configuration to configuration.

These results for the analysis, shown in Figure 5.2, reveal a number of interesting observations. For longitudinal effectiveness, configurations with actuation frequencies near ± 6 Hz are generally seen to experience low to medium value effectiveness. That is because the lower absolute speeds experienced by the legs for such frequencies naturally constrains the amount by which φ can grow. There is one interesting behavior seen for $\alpha = 90°$, where effectiveness drops dramatically upon moving from +7 Hz to +8 Hz. What is particularly interesting is that such a decline is seen even though the respective value of the velocity is fairly comparable. What happens here is revealing: there is seen to be an appreciable spike in sensitivity for $f = 8$ Hz, which implies the gait dynamics is less resilient against surface variation for such an actuation rate.

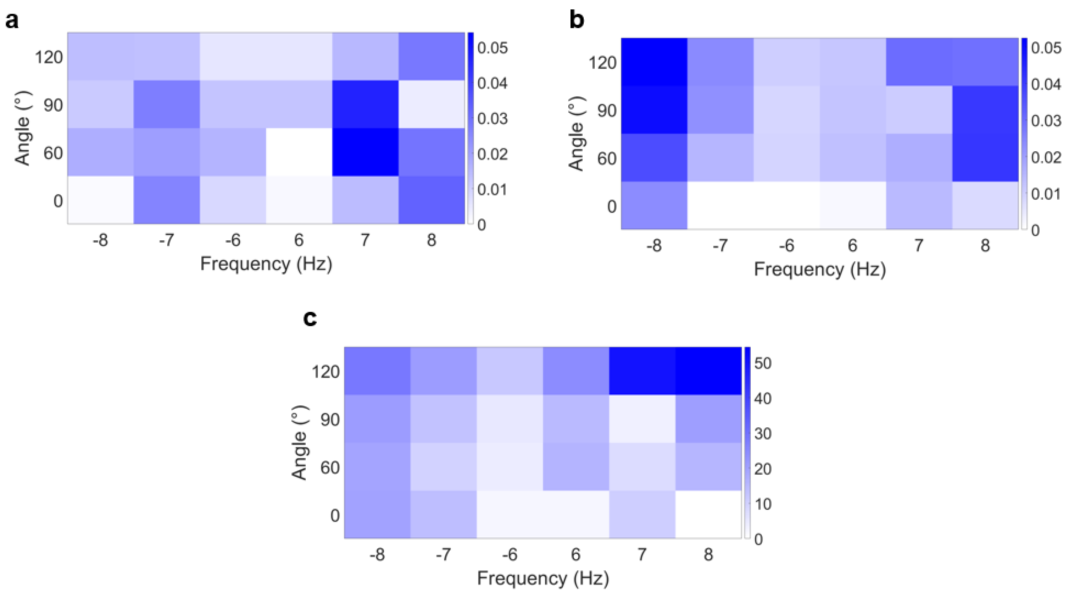

Figure 5.2: Simulated effectiveness analysis. a) Longitudinal, b) lateral, and c) rotational effectiveness assessments for various actuation frequencies (x-axis) and α values (y-axis).

This finding is also illustrated in Figure 5.3 where foot trajectories and gait are contrasted for such two frequencies. In part (a), for the high-effectiveness regime at $f = 7$ Hz, the foot trajectory for the robot is stable for both pre-and post-varying conditions in friction. However, for $f = 8$ Hz, the same value for α produces a foot trajectory which is considerably different for varying conditions for the friction, revealing the configuration's larger sensitivity. Part (b) of the same figure provides more details; the corresponding simulated gait illustrates that for 8 Hz, the right foot for the first module is no longer maintaining contact with the ground. Loss of such ground contact is detrimental for longitudinal propulsion, hence reducing effectiveness. Interestingly enough, such a modification for the contact pattern for the foot has the tendency to improve lateral as well as rotational performance by virtue of added directional mobility alongside reduced ground resistance for rotational motion.

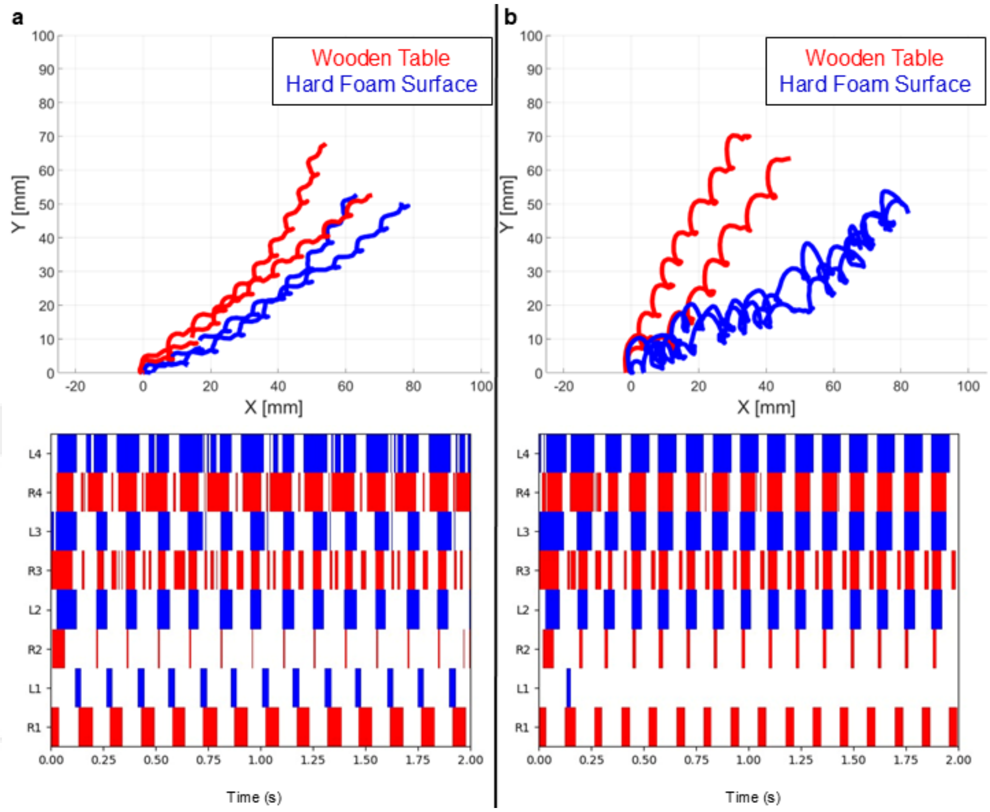

Figure 5.3: Analysis of effectiveness values. a) Trajectory and corresponding gait for $\alpha = 90°$ and $f = 7$ Hz, a configuration associated with high effectiveness. b) Trajectory and corresponding gait for $\alpha = 90°$ and $f = 8$ Hz, a configuration associated with low effectiveness. In both cases, the top panel shows the foot trajectory, while the bottom panel depicts the resulting gait pattern.

For lateral effectiveness, the pattern is more distinct. We observe the effectiveness index generally increases with the actuation frequency magnitude. That is, larger absolute frequencies (in specific cases, ± 8 Hz) lead to more stable and more rapid lateral displacements. That is particularly so for configurations where $\alpha = 90°$ and $\alpha = 120°$, where lateral effectiveness is optimized.

Rotational effectiveness is also more configuration-dependent. i.e., configurations with $\alpha = 120°$ tend to dominate over others for rotational speed and rotational stability. What this asserts is that for this backbone angle, transmission of vibration and resultant body asymmetry is such that rotational motion is maximized the most. The increase in rotational efficacy for this angle is a result of generation of dynamic imbalance as well as resultant torque by anisotropic backbone arrangement.

In general, joint sensitivity and effectiveness analysis allows for a complete characterization of the kinetic motion of the robot. Identifying configurations in which large velocity coincides with low sensitivity allows one to determine optimal regimes for stable multidirectional motion. These conclusions inform not only design choices for this device, but also provide principles for designing new soft systems with excellent performance in the presence of variation in the environment.

Based on the effectiveness analysis, the optimal single-angle configuration for the fastest and most reliable robot locomotion across all directions is $\alpha = 90°$. This configuration provides a strong balance, with high effectiveness in the longitudinal direction, particularly around 7 Hz, supporting reliable forward movement with minimal sensitivity to frictional changes. Additionally, it demonstrates competitive performance in both lateral and rotational directions, making it a desired choice for multi-directional locomotion from the options that our analysis includes.

5.3 Reinforcement Learning-Based Navigation

Achieving reliable and controllable navigation in a 2D plane requires a robot to perform two fundamental maneuvers: straight-line movement and in-place rotation around its center of geometry. When both capabilities are available the robot can access any desired pose, defined as a combination of location and orientation.

From our experimental and simulation results, we observed that the robot's movement path is curved, with its radius of curvature highly dependent on both the actuation frequency and the relative arrangement of the backbones, which is denoted by α. By carefully combining vibrations of equal frequency and opposite sign (e.g., alternating $+F$ and $-F$ for durations t_1 and t_2), it is possible to counteract the net curvature and achieve approximately straight-line motion.

But getting pure rotation about the center of geometry with minimal translational motion is not so simple. In order to achieve such a motion, the robot must achieve torque with zero linear momentum which is not a simple task given the highly coupled nature of the system. Manual tuning of the actuation signal to obtain such motion is not only time consuming but also suboptimal given the nonlinear nature of system response as well as sensitivity.

To cope with this problem, a model-free reinforcement learning (RL) approach was used to learn appropriate control signals for rotation of center of geometry autonomously. Reinforcement learning is a framework where an agent acts in an environment and is given reward-based feedback. The agent's goal is to obtain a policy, a mapping from observations to actions such that reward is maximized in the long term.

5.3.1 Learning Framework and Algorithm Selection

The objective for the RL agent is to control the robot actuation signal (i.e., the speed and direction of the unbalanced mass) so that the robot rotates about a point with a specified angular speed while maintaining the center-of-geometry positional drift to a minimum.

From the available RL algorithms, we selected Proximal Policy Optimization (PPO) due to its stability and efficiency for continuous control issues. PPO belongs to the family of policy gradient methods where the policy is directly optimized by gradient ascent on expected reward. In contrast with typical policy gradient methods which are put into instability by large updates, PPO introduces an alternative objective function which does not create sudden updates to the policy with iterations. That is achieved by clipping the update ratio in the policy so as to maintain the learning process stable and efficient.

PPO optimizes the clipped objective:

$$L^{\text{CLIP}}(\theta) = \mathbb{E}_t \left[\min \left(r_t(\theta)\hat{A}_t, \ \text{clip}(r_t(\theta), 1-\epsilon, 1+\epsilon)\hat{A}_t \right) \right] \tag{5.4}$$

where $r_t(\theta)$ is the ratio between the new and old policy probabilities for a given action, $\hat{A}_t$ is the advantage estimate at time t, and ϵ is a small constant that bounds the update.

We built a custom OpenAI Gym environment using the MuJoCo simulation. The agent observes the position and orientation of the robot and selects an action from a discrete set of frequency values. The PPO implementation is provided by the Stable-Baselines3 library, which offers a reliable and well-documented toolkit for reinforcement learning. The hyperparameters used for training are summarized in Table 5.1.

Table 5.1: Hyperparameters used for PPO training

Parameter	**Value**
Learning rate (`learning_rate`)	3×10^{-4}
Number of steps (`n_steps`)	2048
Batch size (`batch_size`)	64
Discount factor (γ)	0.99
GAE lambda (λ)	0.95
Clip range (`clip_range`)	0.2
Number of epochs (`n_epochs`)	10
Value function coefficient (`vf_coef`)	0.5
Entropy coefficient (`ent_coef`)	0.2

5.3.2 State, Action, and Reward Definition

The observation space is the robot position (x, y) plus orientation angle θ specifying the pose of the center of geometry. The action space is discretized with 10 distinct frequency values spread over positive and negative frequencies in the 6 to 8 Hz magnitude range. These are selected to be distinguishable experimentally as well as robust to noise and fabrication tolerances.

The reward is designed such that it encourages simultaneously big angular speed around the direction of interest and discourages translational movement far from the initial position. That is how the robot achieves the rotation it wants to achieve but does not translate away from where it is intended to go. The reward in each timestep is:

$$R = -\left(\frac{\Delta\theta}{\Delta t} - \omega_{\text{desired}}\right)^2 \cdot k_{\text{rot}} - \left((x - x_i)^2 + (y - y_i)^2\right) \cdot k_{\text{pos}} \tag{5.5}$$

Here, $\Delta\theta/\Delta t$ is the observed angular velocity, ω_{desired} is the target angular velocity (positive for clockwise or negative for counterclockwise rotation), k_{rot} is a scalar weight on the angular velocity term, and k_{pos} penalizes position deviation from the starting point (x_i, y_i).

5.3.3 Training and Results

The reinforcement learning agent learned optimal policies for maximization of reward for clockwise rotation as well as for counterclockwise rotation of the center of geometry. The learned policy consists of oscillatory frequency input signals of $+100°$ for clockwise rotation and $-100°$ for counterclockwise rotation. These input signals comprise fine modulations of the rotational angle of the motor so it creates directional vibrations to achieve controlled rotational motion with minimum translation.

This motion is depicted in Figure 5.4 as the learned frequency profile over time and final robot trajectory. The success of the learned policy illustrates the capabilities of reinforcement learning to discover advanced control strategies for systems with nonlinear, compliant, and vibration-drivent dynamics.

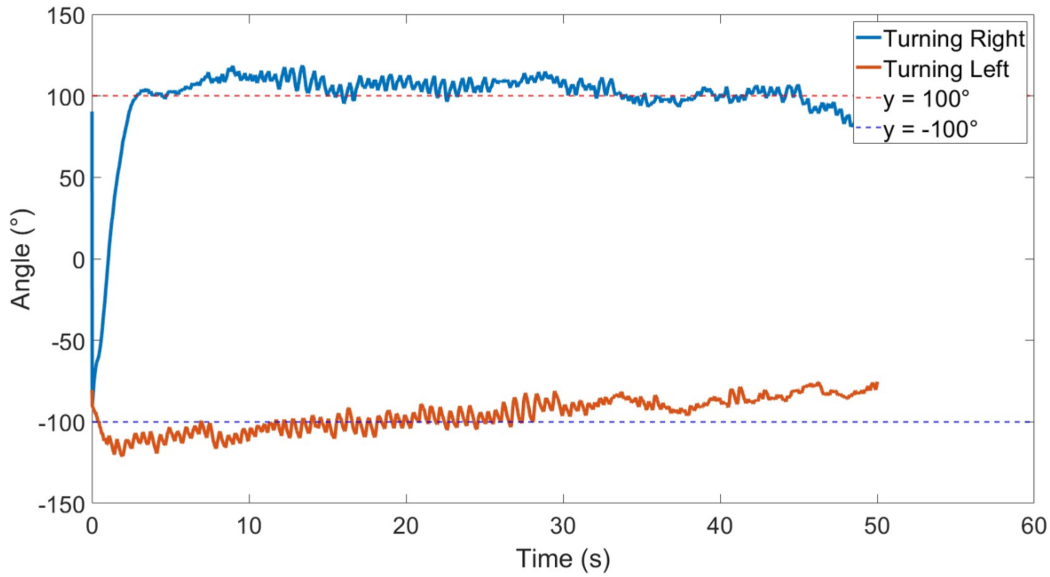

Figure 5.4: Optimal signals for rotation around the center of geometry determined using reinforcement learning for $\alpha = 90$. The y-axis represents the angular position of the mass, corresponding to the control input, while the x-axis denotes time.

5.3.4 Navigation Demonstration

To demonstrate integrated locomotion capabilities, the robot was tasked with navigating a planar maze composed of narrow and sharply turning corridors. The robot used a simple open-loop strategy to move forward by alternating between 7 Hz and –7 Hz inputs, which produced relatively linear motion along the centerline of the maze. Upon encountering a turn too narrow to navigate directly, the control system switched to the reinforcement learning based strategy to rotate the robot around its center of geometry. As captured in the accompanying image sequence in Fig. 5.5, the robot first executes straight motion using open-loop control (frames 1–4). Upon approaching a right-angle turn, it transitions into the RL-based rotation maneuver (frames 4–5), reorients itself precisely, and resumes open-loop navigation (frames 5–7). Later in the sequence, a second learned rotation is performed to negotiate a left turn (frames 7–8), followed by continued forward movement. This sequence validates the robot's ability to integrate learned and handcrafted strategies to achieve reliable navigation with only one actuator and a fixed configuration.

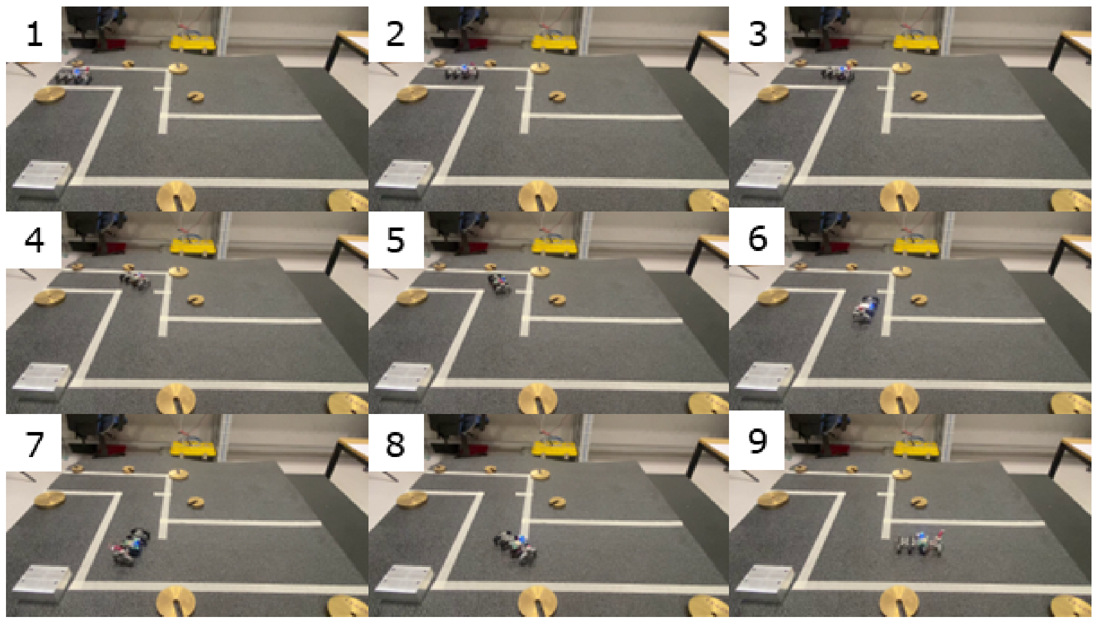

Figure 5.5: A nine-frame sequence illustrating the robot's navigation through a planar maze using a hybrid control strategy. In images 1–4 and 6–7, the robot advances using open-loop straight-path locomotion by alternating between 7 Hz and –7 Hz frequencies. Upon encountering narrow corners, the robot transitions to reinforcement-learning-based rotation maneuvers to realign itself with the path: a right turn in image 5 and a left turn in image 8. Image 9 shows the robot resuming forward motion.

Chapter 6

Conclusion and Future Work

6.1 Conclusion

This thesis proposed the design, modeling, and control for a modular miniature robot actuated by one motor and linked by anisotropically structured soft I-beam backbones. The architecture enables complex and agile gaiting by leveraging the directional compliance of the backbones and switching the actuation frequency using no additional actuators or added mechanics. The minimalist yet feature-packed design demonstrates the potential for combining smart structure with dynamic control for obtaining diversified locomotion behaviors.

A hallmark feature of the design is the inclusion of I-beam-shaped PDMS backbones that create stiffness anisotropy, which by virtue of their relative pose and actuation create motion in the forward direction, lateral motion, as well as rotation. To explore this high-dimensional design space efficiently, the layout of the backbone was parameterized by one angle variable, α. Allowing for such simplification allowed for systematic exploration of an array of configurations experimentally as well as using high-fidelity MuJoCo simulations. The parameter α was varied over a series of actuation frequencies to identify operational regimes which are not just efficient in speed but also robust against variability in friction.

In order to quantify this trade-off between speed and robustness, one measure called the *effectiveness index* was introduced. It combined locomotion speed with a normalized measure of sensitivity to surface friction to provide an objective comparison technique between the robot's performance for varying configurations.

Furthermore, the thesis also explored learning-based control techniques to increase the behavioral capabilities of the robot. The robot was trained using reinforcement learning via the Proximal Policy Optimization algorithm for spinning about the center of geometry while position stable. It was achieved using a MuJoCo-based Gym environment with discretized frequency control as the action space. The resultant policies enabled complex operations such as sharp turns and straight movement using the single actuator. These results demonstrate the potential for combining mechanical intelligence with modern learning algorithms for the creation of goal-oriented systems with less than full actuation.

6.2 Limitations and Future Work

Although the design structure proposed has exhibited promising capabilities via demonstration, there are limitations remaining, which pose potential directions for future work. Firstly, experiments and simulations are carried out on relatively homogeneous surface conditions with minimal controlled variation in the coefficient of friction. But natural environments are more inclined to offer heterogeneous conditions such as inclined planes, soft or deformable substrates, or obstructed terrains. Alleviating such a limitation may require adaptive feedback control mechanisms or designing closed-loop mechanisms based on sensors for stable locomotion performance for diverse conditions.

There is also a significant drawback arising from the simplification of the backbone configuration space. A scalar parameter, α, is employed here for specifying the backbone angles, thereby making it efficient for characterization as well as for analysis. While this approach is experimentally plausible as well as computationally manageable, it inevitably excludes a large class of potentially viable configurations, particularly those with asymmetric or non-linearly connected angles. Extending the configuration space by employing multidimensional parameterizations has the potential for revealing new gait patterns and leg trajectory patterns.

Lastly, the potential system for robots, owing to modularity, low actuation, and mechanically constructed gait generation as foundations, possesses great scaling as well as adaptation potential over a wide range of domains of applications. On small physical scales, the system simplicity of actuation as well as direction compliance might achieve gigantic payoffs in biomedical as well as microrobotic applications, where space as well as power is an essential constraint. On the contrary, scaling the system larger might enable deploying it for more labor-intensive applications like field work during industrial inspection, surveillance, or search-and-rescue operations, where mechanical simplicity, toughness, as well as compliance over terrain are preferred. Future work may explore such choices for scaling as well as modify the system architecture accordingly in order to meet needs by such applications in such diverse environments.

In addition, the reinforcement learning model itself could be employed not only for task-optimized control but also for discovery of novel and heterogenous locomotion strategies. The model, trained with less specific goals or other reward functions, could reveal actuation patterns not crafted by hand—perhaps more efficient, robust, or novel gaits. It could also be used for optimization of robot design parameters, such as the unbalanced mass or robot size, in the hope of attaining a near-optimal design. This would also enable the derivation of adaptive control signals for more challenging tasks in other terrains and constraints.

On the whole, this dissertation demonstrates the viability of obtaining agile movement on highly constrained robotic systems via judiciously designed mechanical structure and learning-based control. Future developments must further improve such capabilities with more robustness, versatility, and functionality.

Bibliography

[1] X. Xia, C. M. Spadaccini, and J. R. Greer, "Responsive materials architected in space and time," *Nature Reviews Materials*, vol. 7, no. 9, pp. 683–701, 2022.

[2] P. Jiao, J. Mueller, J. R. Raney, X. Zheng, and A. H. Alavi, "Mechanical metamaterials and beyond," *Nature communications*, vol. 14, no. 1, p. 6004, 2023.

[3] S. Shen, X. Liu, Y. Shen, J. Qu, E. Pickwell-MacPherson, X. Wei, and Y. Sun, "Recent advances in the development of materials for terahertz metamaterial sensing," *Advanced Optical Materials*, vol. 10, no. 1, p. 2101008, 2022.

[4] S. Bonfanti, R. Guerra, F. Font-Clos, D. Rayneau-Kirkhope, and S. Zapperi, "Automatic design of mechanical metamaterial actuators," *Nature communications*, vol. 11, no. 1, p. 4162, 2020.

[5] X. Zheng, K. Uto, W.-H. Hu, T.-T. Chen, M. Naito, and I. Watanabe, "Reprogrammable flexible mechanical metamaterials," *Applied Materials Today*, vol. 29, p. 101662, 2022.

[6] D. Li, S. Huang, Y. Tang, H. Marvi, J. Tao, and D. M. Aukes, "Compliant fins for locomotion in granular media," *IEEE Robotics and Automation Letters*, vol. 6, no. 3, pp. 5984–5991, 2021.

[7] S. Chopra, D. Vasile, S. Jadhav, M. T. Tolley, and N. Gravish, "Toward robotic sensing and swimming in granular environments using underactuated appendages," *Advanced Intelligent Systems*, vol. 5, no. 8, p. 2200404, 2023.

[8] W. Xu, H. Zhang, H. Yuan, and B. Liang, "A compliant adaptive gripper and its intrinsic force sensing method," *IEEE Transactions on Robotics*, vol. 37, no. 5, pp. 1584–1603, 2021.

[9] T. Wu, Z. Liu, B. Wang, Z. Ma, D. Ma, and X. Deng, "A versatile topology-optimized compliant actuator for soft robotic gripper and walking robot," *Soft Robotics*, vol. 11, no. 1, pp. 157–170, 2024.

[10] A. Zolfagharian, S. Gharaie, J. Gregory, M. Bodaghi, A. Kaynak, and S. Nahavandi, "A bioinspired compliant 3d-printed soft gripper," *Soft Robotics*, vol. 9, no. 4, pp. 680–689, 2022.

[11] Z. Zhai, Y. Wang, K. Lin, L. Wu, and H. Jiang, "In situ stiffness manipulation using elegant curved origami," *Science advances*, vol. 6, no. 47, p. eabe2000, 2020.

[12] A. Maruo, A. Shibata, and M. Higashimori, "Dynamic underactuated manipulator using a flexible body with a structural anisotropy," in *2022 International Conference on Robotics and Automation (ICRA)*, pp. 7117–7123, IEEE, 2022.

[13] G. Bledt, M. J. Powell, B. Katz, J. Di Carlo, P. M. Wensing, and S. Kim, "Mit cheetah 3: Design and control of a robust, dynamic quadruped robot," in *2018 IEEE/RSJ International Conference on Intelligent Robots and Systems (IROS)*, pp. 2245–2252, IEEE, 2018.

[14] M. Hutter, C. Gehring, D. Jud, A. Lauber, C. D. Bellicoso, V. Tsounis, J. Hwangbo, K. Bodie, P. Fankhauser, M. Bloesch, *et al.*, "Anymal-a highly mobile and dynamic quadrupedal robot," in *2016 IEEE/RSJ international conference on intelligent robots and systems (IROS)*, pp. 38–44, IEEE, 2016.

[15] M. Raibert, K. Blankespoor, G. Nelson, and R. Playter, "Bigdog, the rough-terrain quadruped robot," *IFAC Proceedings Volumes*, vol. 41, no. 2, pp. 10822–10825, 2008.

[16] A. Badri-Spröwitz, A. Aghamaleki Sarvestani, M. Sitti, and M. A. Daley, "Birdbot achieves energy-efficient gait with minimal control using avian-inspired leg clutching," *Science Robotics*, vol. 7, no. 64, p. eabg4055, 2022.

[17] S. Kim, J. E. Clark, and M. R. Cutkosky, "isprawl: Design and tuning for high-speed autonomous open-loop running," *The International Journal of Robotics Research*, vol. 25, no. 9, pp. 903–912, 2006.

[18] U. Saranli, M. Buehler, and D. E. Koditschek, "Rhex: A simple and highly mobile hexapod robot," *The International Journal of Robotics Research*, vol. 20, no. 7, pp. 616–631, 2001.

[19] A. T. Baisch, O. Ozcan, B. Goldberg, D. Ithier, and R. J. Wood, "High speed locomotion for a quadrupedal microrobot," *The International Journal of Robotics Research*, vol. 33, no. 8, pp. 1063–1082, 2014.

[20] K. L. Hoffman and R. J. Wood, "Robustness of centipede-inspired millirobot locomotion to leg failures," in *2013 IEEE/RSJ International Conference on Intelligent Robots and Systems*, pp. 1472–1479, IEEE, 2013.

[21] P. Birkmeyer, K. Peterson, and R. S. Fearing, "Dash: A dynamic 16g hexapedal robot," in *2009 IEEE/RSJ international conference on intelligent robots and systems*, pp. 2683–2689, IEEE, 2009.

[22] M. Agheli, S. G. Faal, F. Chen, H. Gong, and C. D. Onal, "Design and fabrication of a foldable hexapod robot towards experimental swarm applications," in *2014 IEEE International Conference on Robotics and Automation (ICRA)*, pp. 2971–2976, IEEE, 2014.

[23] D. Feshbach, X. Wu, S. Vasireddy, L. Beardell, B. To, Y. Baryshnikov, and C. Sung, "Curvequad: a centimeter-scale origami quadruped that leverages curved creases to self-fold and crawl with one motor," in *2023 IEEE/RSJ International Conference on Intelligent Robots and Systems (IROS)*, pp. 2485–2492, IEEE, 2023.

[24] P. A. Bhounsule, J. Cortell, A. Grewal, B. Hendriksen, J. D. Karssen, C. Paul, and A. Ruina, "Low-bandwidth reflex-based control for lower power walking: 65 km on a single battery charge," *The International Journal of Robotics Research*, vol. 33, no. 10, pp. 1305–1321, 2014.

[25] S. Islam, K. Carter, J. Yim, J. Kyle, S. Bergbreiter, and A. M. Johnson, "Scalable minimally actuated leg extension bipedal walker based on 3d passive dynamics," in *2022 International Conference on Robotics and Automation (ICRA)*, pp. 207–213, IEEE, 2022.

[26] J. G. Cham, S. A. Bailey, J. E. Clark, R. J. Full, and M. R. Cutkosky, "Fast and robust: Hexapedal robots via shape deposition manufacturing," *The International Journal of Robotics Research*, vol. 21, no. 10-11, pp. 869–882, 2002.

[27] M. Jiang, Z. Zhou, and N. Gravish, "Flexoskeleton printing enables versatile fabrication of hybrid soft and rigid robots," *Soft robotics*, vol. 7, no. 6, pp. 770–778, 2020.

[28] H. H. Hariri, L. A. Prasetya, S. Foong, G. S. Soh, K. N. Otto, and K. L. Wood, "A tether-less legged piezoelectric miniature robot using bounding gait locomotion for bidirectional motion," in *2016 IEEE International Conference on Robotics and Automation (ICRA)*, pp. 4743–4749, IEEE, 2016.

[29] L. Tang, C. Wang, S. Ma, Y. Li, and B. Li, "Multidirectional planar motion transmission on a single-motor actuated robot via microscopic galumphing," *Advanced Science*, vol. 11, no. 9, p. 2307738, 2024.

[30] M. Rubenstein, C. Ahler, and R. Nagpal, "Kilobot: A low cost scalable robot system for collective behaviors," in *2012 IEEE international conference on robotics and automation*, pp. 3293–3298, IEEE, 2012.

[31] Y. Zhu, M. Qi, Z. Liu, J. Huang, D. Huang, X. Yan, and L. Lin, "A 5-mm untethered crawling robot via self-excited electrostatic vibration," *IEEE Transactions on Robotics*, vol. 38, no. 2, pp. 719–730, 2021.

[32] T. Li, Z. Zou, G. Mao, X. Yang, Y. Liang, C. Li, S. Qu, Z. Suo, and W. Yang, "Agile and resilient insect-scale robot," *Soft robotics*, vol. 6, no. 1, pp. 133–141, 2019.

[33] Y. Yan, L. Shui, S. Liu, Z. Liu, and Y. Liu, "Terrain adaptability and optimum contact stiffness of vibro-bot with arrayed soft legs," *Soft Robotics*, vol. 9, no. 5, pp. 981–990, 2022.

[34] K. Johnson, Z. Englhardt, V. Arroyos, D. Yin, S. Patel, and V. Iyer, "Millimobile: An autonomous battery-free wireless microrobot," in *Proceedings of the 29th Annual International Conference on Mobile Computing and Networking*, pp. 1–16, 2023.

[35] Y. Jiang, M. Sharifzadeh, and D. M. Aukes, "Reconfigurable soft flexure hinges via pinched tubes," in *2020 IEEE/RSJ International Conference on Intelligent Robots and Systems (IROS)*, pp. 8843–8850, IEEE, 2020.

[36] Y. Jiang, M. Sharifzadeh, and D. M. Aukes, "Shape change propagation through soft curved materials for dynamically-tuned paddling robots," in *2021 IEEE 4th International Conference on Soft Robotics (RoboSoft)*, pp. 230–237, IEEE, 2021.

[37] M. Jiang, Q. Yu, and N. Gravish, "Vacuum induced tube pinching enables reconfigurable flexure joints with controllable bend axis and stiffness," in *2021 IEEE 4th International Conference on Soft Robotics (RoboSoft)*, pp. 315–320, IEEE, 2021.

[38] M. Sharifzadeh and D. M. Aukes, "Curvature-induced buckling for flapping-wing vehicles," *IEEE/ASME Transactions on Mechatronics*, vol. 26, no. 1, pp. 503–514, 2020.

[39] M. Sharifzadeh, Y. Jiang, and D. M. Aukes, "Reconfigurable curved beams for selectable swimming gaits in an underwater robot," *IEEE Robotics and Automation Letters*, vol. 6, no. 2, pp. 3437–3444, 2021.

[40] Y. Jiang, F. Chen, and D. M. Aukes, "Tunable dynamic walking via soft twisted beam vibration," *IEEE Robotics and Automation Letters*, vol. 8, no. 4, pp. 1967–1974, 2023.

[41] E. Todorov, T. Erez, and Y. Tassa, "Mujoco: A physics engine for model-based control," in *2012 IEEE/RSJ International Conference on Intelligent Robots and Systems*, pp. 5026–5033, 2012.